



# Infectious Bursal Disease Virus Hijacks Endosomal Membranes as the Scaffolding Structure for Viral Replication

María Cecilia Gimenez,<sup>a,c</sup> Flavia Adriana Zanetti,<sup>d</sup> Mauricio R. Terebiznik,<sup>e,f</sup> María Isabel Colombo,<sup>a</sup> Laura Ruth Delgui<sup>a,b</sup>

<sup>a</sup>IHEM, Universidad Nacional de Cuyo, CONICET, Facultad de Ciencias Médicas, Mendoza, Argentina

<sup>b</sup>Facultad de Ciencias Exactas y Naturales, Universidad Nacional de Cuyo, Mendoza, Argentina

<sup>c</sup>Facultad de Ciencias Veterinarias y Ambientales, Universidad Juan Agustín Maza, Mendoza, Argentina

<sup>d</sup>Instituto de Ciencia y Tecnología Dr. Cesar Milstein, Consejo Nacional de Investigaciones Científicas y Técnicas, Buenos Aires, Argentina

<sup>e</sup>Department of Biological Sciences, University of Toronto at Scarborough, Scarborough, Scarborough, Canada

<sup>f</sup>Department of Cell and System Biology, University of Toronto at Scarborough, Scarborough, Scarborough, Canada

**ABSTRACT** Birnaviruses are unconventional members of the group of double-stranded RNA (dsRNA) viruses that are characterized by the lack of a transcriptionally active inner core. Instead, the birnaviral particles organize their genome in ribonucleoprotein complexes (RNPs) composed by dsRNA segments, the dsRNA-binding VP3 protein, and the virally encoded RNA-dependent RNA polymerase (RdRp). This and other structural features suggest that birnaviruses may follow a completely different replication program from that followed by members of the *Reoviridae* family, supporting the hypothesis that birnaviruses are the evolutionary link between single-stranded positive RNA (+ssRNA) and dsRNA viruses. Here we demonstrate that infectious bursal disease virus (IBDV), a prototypical member of the *Birnaviridae* family, hijacks endosomal membranes of infected cells through the interaction of a viral protein, VP3, with the phospholipids on the cytosolic leaflet of these compartments for replication. Employing a mutagenesis approach, we demonstrated that VP3 domain PATCH 2 (P2) mediates the association of VP3 with the endosomal membranes. To determine the role of VP3 P2 in the context of the virus replication cycle, we used avian cells stably overexpressing VP3 P2 for IBDV infection. Importantly, the intra- and extracellular virus yields, as well as the intracellular levels of VP2 viral capsid protein, were significantly diminished in cells stably overexpressing VP3 P2. Together, our results indicate that the association of VP3 with endosomes has a relevant role in the IBDV replication cycle. This report provides direct experimental evidence for membranous compartments such as endosomes being required by a dsRNA virus for its replication. The results also support the previously proposed role of birnaviruses as an evolutionary link between +ssRNA and dsRNA viruses.

**IMPORTANCE** Infectious bursal disease (IBD; also called Gumboro disease) is an acute, highly contagious immunosuppressive disease that affects young chickens and spreads worldwide. The etiological agent of IBD is infectious bursal disease virus (IBDV). This virus destroys the central immune organ (bursa of Fabricius), resulting in immunosuppression and reduced responses of chickens to vaccines, which increase their susceptibility to other pathogens. IBDV is a member of *Birnaviridae* family, which comprises unconventional members of dsRNA viruses, whose replication strategy has been scarcely studied. In this report we show that IBDV hijacks the endosomes of the infected cells for establishing viral replication complexes via the association of the ribonucleoprotein complex component VP3 with the phospholipids in the cytosolic leaflet of endosomal membranes. We show that this interaction is me-

Received 12 November 2017 Accepted 8 February 2018

Accepted manuscript posted online 14 March 2018

**Citation** Gimenez MC, Zanetti FA, Terebiznik MR, Colombo MI, Delgui LR. 2018. Infectious bursal disease virus hijacks endosomal membranes as the scaffolding structure for viral replication. *J Virol* 92:e01964-17. <https://doi.org/10.1128/JVI.01964-17>.

**Editor** Susana López, Instituto de Biotecnología/UNAM

**Copyright** © 2018 American Society for Microbiology. All Rights Reserved.

Address correspondence to Laura Ruth Delgui, [ldelgui@fcm.uncu.edu.ar](mailto:ldelgui@fcm.uncu.edu.ar).

diated by the VP3 PATCH 2 domain and demonstrate its relevant role in the context of viral infection.

**KEYWORDS** +ssRNA, birnavirus, endosomes, Gumboro disease, virus replication complex

**R**NA viruses replicate within the cytoplasm of host cells via RNA intermediates. Their genome is either single-stranded, positive- or negative-strand RNA (+ssRNA or –ssRNA, respectively) or double-stranded RNA (dsRNA). In spite of these differences in genome composition, their replication requires the formation of intermediate dsRNA molecules that can be detected by intracellular sensor triggering antiviral responses. To escape surveillance receptors, +ssRNA viruses generate and replicate associated with rearrangements of specific intracellular membranes (recently reviewed in reference 1).

On the other hand, dsRNA viruses, including the prototypical rota-, reo-, and orbiviruses of the *Reoviridae* family, which are relevant human, animal and plant pathogens, follow a different replication strategy. They are composed by a multilayered concentric icosahedral capsid (2), where the innermost layer has a unique T=1 icosahedral organization termed the transcriptional core, essential for genome and replication complex organization (3). The transcriptional core remains intact throughout the replication cycle, hiding newly generated dsRNA molecules and thus preventing their detection by host surveilling mechanisms (4, 5).

Infectious bursal disease virus (IBDV) is the best-characterized member of the *Birnaviridae* family. IBDV is an avibirnavirus and the etiological agent of infectious bursal disease (IBD; Gumboro disease), an immunosuppressive condition in chickens, in which IBDV infects and destroys immature B lymphocytes in the bursa of Fabricius. The severity of IBD depends on the virulence of the viral strain, as well as the age and breed of chickens (6). First described in the United States in 1962 (7), IBD is now present worldwide and a relevant economic burden for the poultry industry.

IBDV virions are nonenveloped icosahedral capsids formed by pentameric and hexameric arrangements of the protein VP2, with a triangulation number of T=13 and a diameter of ~70 nm (8, 9). We have previously shown that upon adsorption and receptor recognition, the viral particles hijack the macropinocytic pathway for internalization, traffic to endosomes in a Rab5-dependent manner, and take advantage of their acidification to infect the host cells (10). We have also demonstrated, by assessing the cellular distribution of the ribonucleoprotein complex (RNP) components, VP3, the RNA-dependent RNA polymerase (RdRp), and the dsRNA, that IBDV replication requires association with endosomes and proved a role for the Golgi complex in IBDV assembly (11).

IBDV contains a polytypic bipartite genome composed by segment A, which includes two partially overlapping open reading frames (ORFs). The first ORF encodes the nonessential nonstructural viral protein 5 (VP5), involved in nonlytic egression of IBDV particles (12). The second ORF encodes a polyprotein that is cotranslationally autocleaved by the viral protease VP4, generating the precursor pVP2, VP4, and VP3 (13). The resulting intermediate, pVP2, is further processed at the C-terminal region by both VP4 and puromycin-sensitive aminopeptidase (PurSA) to generate the mature VP2 (14, 15). The VP2 maturation process generates several peptides that remain associated with the capsid and contribute to the perforation of endosomes (16, 17). VP2 and VP3 are the major structural proteins in IBDV, constituting 60% and 35% of the virion, respectively (18). Segment B, the shorter segment in the IBDV genome, is monocistronic and encodes the viral RdRp termed VP1 (19).

Birnaviruses lack the T=2 core, which is structurally conserved in dsRNA viruses. Instead, their genomes are integrated into RNPs consisting of VP1-dsRNA, dsRNA-unbound VP1 (free VP1), and VP3 (18). These RNPs are fully capable of initiating a productive IBDV replication process (20), similar to the replication and transcription complexes of some +ssRNA viruses (21, 22). VP3 (258 amino acid residues and 32 kDa) is a multitasking protein that is able to undergo homotypic interactions (23, 24) and, as

well, interact with either pVP2 (25, 26) or VP1 (24, 27, 28). Furthermore, VP3 plays a role in both virus replication and morphogenesis. For replication, the VP3 C terminus acts as an RdRp transcriptional activator (27) and a suppressor of the RNA silencing machinery (29, 30). During morphogenesis, VP3 acts as a scaffolding protein and coassembles with pVP2 for capsid assembly (25) and recruits VP1 and the viral genome for encapsidation.

In this work, we aimed at studying the endocytic structures as the membranous scaffold for IBDV replication, with a focus on the role of VP3 in this process. We demonstrated that following viral uncoating, the capsid protein VP2 undergoes lysosomal degradation, while VP3 mediates the association of the viral replication complexes to phospholipids at the cytosolic face of endosomal membranes. Moreover, we identified the VP3 domain that mediates this association and determined its role in the IBDV replication cycle. Together our results are the first direct experimental evidence for membranous compartments such as endosomes being required by a dsRNA virus for its replication. Indeed, results presented here support the previously proposed role of birnaviruses as an evolutionary link between +ssRNA and dsRNA viruses.

## RESULTS

**IBDV capsid protein VP2 undergoes lysosomal degradation after virus disassembly.** Recently, Galloux and collaborators elegantly demonstrated that PEP46, one of the four characteristic peptides generated during VP2 maturation, is exposed at low calcium concentrations and has the capacity to deform biological membranes leading to the formation of pores. Accordingly, they suggested a model in which the reduction of endosomal calcium concentration associated with the endosomal maturation process ( $\text{Ca}^{2+}$ : 3 to 30  $\mu\text{M}$  [31, 32]) causes conformational changes in the capsid, exposing multiple molecules of PEP46, leading to membrane deformation and the perforation of endosomes (17, 31). Thus, considering this model, we hypothesized that after being internalized by macropinocytosis and reaching acidic, low- $\text{Ca}^{2+}$ , Rab5-containing endosomes, capsids disassemble and expose several copies of PEP46 able to generate pores on endosomal membranes. The remaining disassembled VP2 proteins undergo lysosomal degradation while the RNPs extrude through the pores, localize to naive endosomes, and start replication.

In order to test our hypothesis, we investigated the fate of VP2 and VP3 in QM7 cells infected by IBDV at different times postinternalization. For this purpose, two different sets of QM7 cells were cultured and either mock treated or infected with IBDV at a multiplicity of infection (MOI) of 3 (one set). Following virus internalization, the inoculum medium was replaced with fresh culture medium.

Our results indicate that the relative levels of VP2 showed a significant decrease at 2 and 4 h postinfection (p.i.), followed by a recovery of VP2. The latter was also accompanied by an accumulation of VP3 after 8 h p.i. Importantly, this indicates a bifurcated pathway for the capsid VP2 proteins and the VP3-containing RNPs, occurring early after viral uncoating in endosomes (Fig. 1A).

With the aim of verifying the lysosomal activity on VP2 proteins, we analyzed the fate of VP2 and VP3 in IBDV-infected QM7 cells employing bafilomycin A1 (BafA1), which specifically inhibits the proton pump ( $\text{H}^{+}$ -ATPase) responsible for intravesicular acidification and lysosomal protein degradation (32, 33). First, we tested BafA1 treatment by assessing the lysosomal degradation of LC3-II in autophagosomes, which depends on lysosomal activity and has been previously reported to be disrupted by BafA1, causing an increase in the relative levels of both LC3-I precursor and LC3-II (34–36). Accordingly, we observed an increase in LC3-I and LC3-II after BafA1 treatment of QM7 cells (data not shown). Next, four different sets of QM7 cells were cultured and infected with IBDV at an MOI of 3. After virus internalization, infection medium was replaced with fresh culture medium. One of the sets was treated with BafA1 1 h p.i. for 3 h in order to assess VP2 and VP3 levels in the infected cells at 4 h p.i. We also assessed VP2 and VP3 levels in BafA1-treated cells at 4 h p.i., because we obtained the lowest VP2 level at that time point (Fig. 1A). Our results depicted in Fig. 1B show that BafA1 treatment produced a significant accumulation of VP2 compared with the control,

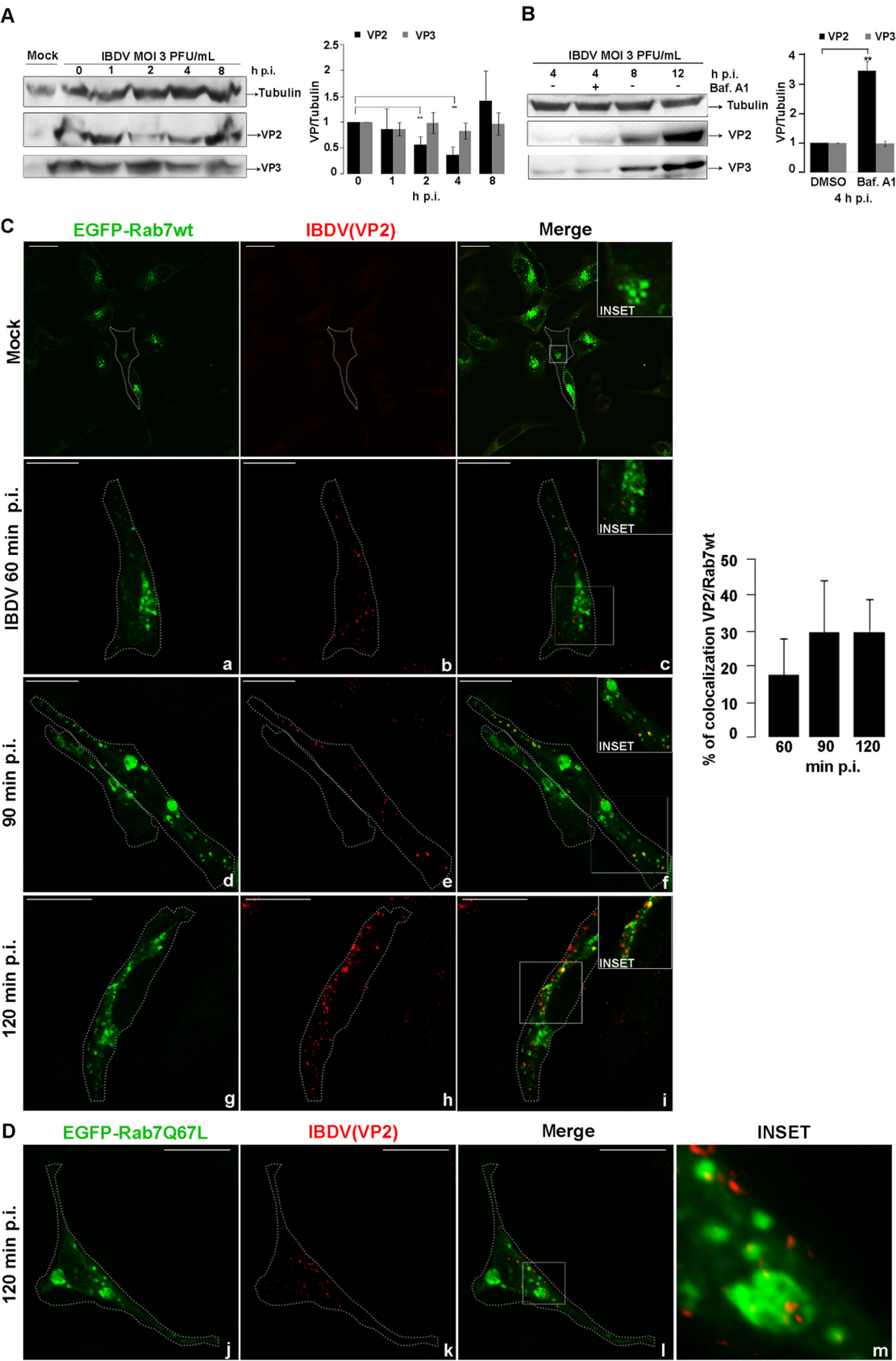


**FIG 1** Fate of the viral capsid protein VP2 following virus internalization. (A) VP2 and VP3 detection in infected cells after virus entry. QM7 cells were grown in an M6 multiwell plate to approximately 70% confluence and infected with IBDV Soroa at an MOI of 3 PFU/ml (Continued on next page)

followed by an increase in VP2 levels at 8 and 12 h p.i. In contrast, VP3 remained stable at 4 h p.i., with an appreciable accumulation of the protein after 8 and 12 h p.i. These results further support a bifurcated pathway followed by the capsid VP2 proteins and the VP3-containing RNPs after viral uncoating in endosomes (Fig. 1B).

To further test the possibility that following virus internalization, VP2 polypeptides were lysosomally degraded, we analyzed the colocalization of VP2 with Rab7, a Rab protein specifically associated with degradative compartments, late endosomes, and lysosomes (37). QM7 cells transiently overexpressing wild-type Rab7 tagged with enhanced green fluorescent protein (EGFP-Rab7 wt) were mock infected or infected with IBDV at an MOI of 10, and at 60, 90, or 120 min p.i., the infected cells were processed for indirect immunofluorescence (IFI) using anti-VP2 antibodies and analyzed by confocal laser scanning microscopy (CLSM). We observed an increasing colocalization between the EGFP-Rab7 wt and VP2 proteins, which reached its maximum at 2 h p.i. (120 min), reinforcing the notion of VP2 proteins trafficking to late compartments (Fig. 1C). Similarly, as depicted in Fig. 1D, QM7 cells transiently overexpressing EGFP-Rab7-Q67L, a constitutively active mutant of Rab7 that stimulates early to late endosomal transport (38), showed an accumulation of VP2 proteins. Together, these results reinforce the notion that VP2 from disassembled viral capsid is degraded in lysosomes while replication complexes become associated with naive early endosomal compartments.

**IBDV multitasking protein VP3 binds to the cytosolic leaflet of endosomal membranes.** In our previous work, we reported that recombinant VP3, expressed in the absence of other viral elements, localized to endosomal compartments, suggesting that VP3 is responsible for targeting the replication machinery to endosomes in infected cells (11). To further explore the mechanism that underlies the association of VP3 with endosomal compartments, we analyzed the morphology of VP3 association with endosomes. To do this, we employed transient overexpression of EGFP-Rab5 wt and a constitutively active mutant of Rab5 protein, EGFP-Rab5-Q79L. Rab5 regulates the homotypic tethering and fusion of early endosomes and is considered a genuine marker of early endosomes (39). Moreover, overexpression of EGFP-Rab5-Q79L induces the formation of enlarged Rab5-positive vesicles that fail to undergo further maturation (40). Thus, QM7 cells transiently overexpressing EGFP-Rab5 wt or EGFP-Rab5-Q79L were infected with IBDV strain Soroa at an MOI of 1 PFU/cell, and at 24 h p.i., the cells were processed for IFI analysis using anti-VP3 antibodies and analyzed by CLSM. As shown in Fig. 2A, VP3 presented a punctate distribution with a marked colocalization with Rab5 wt (top row). However, in EGFP-Rab5-Q79L-overexpressing cells, we observed a patchy distribution pattern of VP3 associated with the endosomal membranes (Fig. 2A, bottom row). Next, we aimed to elucidate the topology of VP3 association with endosomal

#### FIG 1 Legend (Continued)

or incubated in virus-free culture medium (mock-infected cells). After virus internalization, the medium was replaced with fresh culture medium and the relative amounts of VP2 and VP3 viral proteins were analyzed at 1, 2, 4, and 8 h p.i. by Western blotting, as described in Materials and Methods. Corresponding horseradish peroxidase (HRP)-conjugated anti-mouse and anti-rabbit secondary antibodies were used to detect immunoreactive bands by chemiluminescence. The data shown in the normalized bar graph correspond to an experiment representing three independent trials (\*\*,  $P < 0.05$ ). Error bars show SD. (B) QM7 cells were grown in an M6 multiwell plate to approximately 70% confluence and infected with IBDV Soroa at an MOI of 3 PFU/ml. After virus internalization, the medium was replaced with fresh culture medium and 1  $\mu$ l of dimethyl sulfoxide (DMSO) or 10 nM BafA1 was added at 1 h p.i. in the corresponding wells. The relative amounts of VP2 and VP3 viral proteins were analyzed at 4, 8, and 12 h p.i. by Western blotting as described in Materials and Methods. Corresponding HRP-conjugated anti-mouse and anti-rabbit secondary antibodies were used to detect immunoreactive bands by chemiluminescence. The data shown in the normalized bar graph correspond to an experiment representing two independent trials (\*\*,  $P < 0.05$ ). Error bars show SD. R.U., relative units. (C) Intracellular trafficking of VP2 after virus internalization. QM7 cells transfected with a GFP-tagged form of wild-type Rab7 were infected with IBDV Soroa at an MOI of 10 PFU/ml or incubated in virus-free culture medium (mock-infected cells) and at 60, 90, and 120 min p.i. were processed for indirect immunofluorescence using anti-VP2 primary antibodies and the corresponding Cy3-conjugated secondary antibodies. Shown are representative images from a time course colocalization analysis between specific VP2 signals and EGFP-Rab7 wt (a to i). Colocalization analysis was performed employing ImageJ software, analyzing 30 cells per condition. Data are represented as means  $\pm$  SD. Scale bars represent 10  $\mu$ m. (D) The accumulation of specific VP2 signal inside large late endosomes. QM7 cells transfected with a GFP-tagged form of a constitutively active mutant, Rab7-Q67L, were infected with IBDV Soroa at an MOI of 10 PFU/ml or incubated in virus-free culture medium (mock-infected cells) and at 120 min p.i. were processed for indirect immunofluorescence as described for panel C. Scale bars represent 10  $\mu$ m.

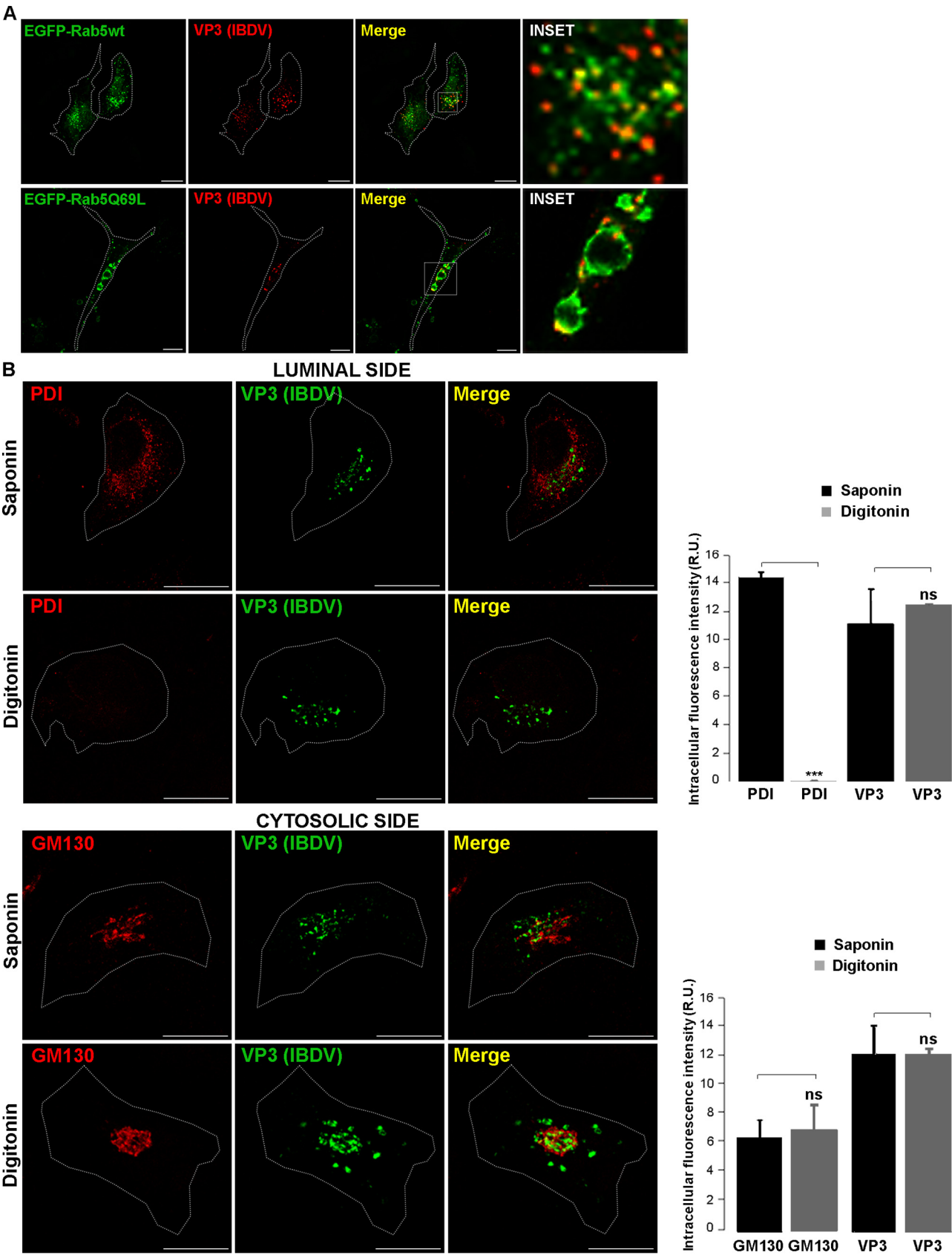


**FIG 2** Characterization of the association of VP3 polypeptide with endosomal compartments. (A) Morphology of VP3 association with endosomes. EGFP-Rab5 wt or a constitutively active mutant of Rab5 protein, EGFP-Rab5-Q79L, were transiently overexpressed in QM7 cells, which were then infected

(Continued on next page)

membranes in the context of the viral infection. Therefore, we performed a differential permeabilization approach which is widely used to study membrane protein topology. This is based on the employment of two permeabilization agents: digitonin, which under specific conditions selectively permeabilizes the plasma membrane, and saponin, which permeabilizes all cellular membranes (41–45). To control the selective permeabilization, we assessed the accessibility of the endoplasmic reticulum (ER) protein disulfide isomerase (PDI) to immunofluorescence antibodies in digitonin- or saponin-treated cells. PDI, which is widely used as luminal marker in selective permeabilization protocols, is the first discovered, most abundant, and best-characterized oxidoreductase within the ER (46–49). Since the antibodies against PDI did not recognize the avian protein, we used HeLa cells, which are permissive to IBDV infection, instead of QM7 cells. Figure 2 shows that while PDI depicted a typical ER staining pattern in saponin-permeabilized HeLa cells (Fig. 2B, top saponin row), this was not the case for digitonin-permeabilized cells (Fig. 2B, bottom digitonin row). These results are consistent with digitonin failing to permeabilize the ER membrane under our experimental conditions. On the other side, we employed antibodies against Golgi Matrix 130 protein (GM130) to evaluate the extent of permeabilization by both agents. GM130 is a peripheral membrane protein tightly bound to the cytoplasmic side of the *cis*-Golgi complex (50, 51). As expected, we observed IFI signal of GM130 after both types of permeabilization (Fig. 2B, bottom rows). Subsequently, HeLa cells were infected with IBDV at an MOI of 1 PFU/cell and at 24 h p.i., the cells were processed for IFI analysis using anti-VP3 antibodies and analyzed by CLSM. As shown in Fig. 2B, punctate distribution of VP3 was observed after treatment with either permeabilization agent. In good agreement with our aforementioned hypothesis that VP3 associates with the cytoplasmic leaflet of naive endosomes, the bar graph in Fig. 2B demonstrates only a small, insignificant difference in VP3 intracellular fluorescence intensity (relative units) in digitonin- or saponin-permeabilized cells, quantitatively suggesting its localization in the cytosolic leaflet of endosomes in infected cells.

**Phosphoinositide binding capacity of VP3 polypeptide.** VP3 viral polypeptide is a moonlighting protein with a highly hydrophilic C-terminal tail region rich in charged amino acids and proline residues that accomplishes several tasks during viral replication and morphogenesis (52). In order to understand the mechanism of VP3-endosomal membrane association, the amino acid sequence of the VP3 polypeptide from IBDV strain Soroa was scanned for conserved domains and/or posttranslational modification that could potentially be responsible for its location at endosomes, expressed either from a recombinant construction or in the context of viral infection. However, none of these putative sites were found in the VP3 nucleotide sequence (data not shown). Finally, since the interaction of small clusters of positively charged amino acids on proteins with negatively charged lipids in membranes constitutes a hallmark in the field of protein-membrane interactions (53), we investigated the presence of polybasic clusters in the protein sequence of VP3 using BioEdit software (54). Interestingly, we found several positively charged amino acid residues, lysine (K) and arginine (R), spread over the VP3 sequence, with a conspicuous predominance at the C-terminal region of VP3, which could be involved in membrane interactions (Fig. 3A). In view of this observation, it was important to assess the capacity of the VP3 polypeptide to interact

## FIG 2 Legend (Continued)

with IBDV Soroa at an MOI of 1 PFU/cell and processed for indirect immunofluorescence analysis at 24 h p.i. using anti-VP3 primary antibodies and Cy3-conjugated secondary antibodies to analyze the VP3 distribution by CLSM. Insets show areas of colocalization between VP3-derived signal and Rab5-positive vesicles (EGFP-derived signal). The images correspond to an experiment representing three independent trials. Scale bars represent 10  $\mu$ m. (B) Topology of VP3 association with endosomes. HeLa cells were infected with IBDV Soroa at an MOI of 1 PFU/cell and processed for indirect immunofluorescence analysis at 24 h p.i. Anti-GM130 and anti-PDI primary antibodies followed by the corresponding Cy3-conjugated secondary antibodies were used as controls of complete permeabilization after saponin treatment or membrane permeabilization after digitonin treatment, respectively. Anti-VP3 primary antibodies followed by Alexa Fluor 488-conjugated secondary antibodies were used to detect the IBDV VP3 protein. Analysis was performed by CLSM. The data shown in the fluorescence images correspond to an experiment representing three independent trials. Scale bars represent 10  $\mu$ m. The intracellular fluorescence intensity was measured using ImageJ software and is represented in bar graphs. Error bars show SD. Thirty cells per condition were scored for each experiment. \*\*\*,  $P < 0.01$ . ns, not significant.

A VP3 (IBDV Soroa strain)

<sup>1</sup> ASEFKETPEL ESAVRAMEAA ANVDPLFQSA LSVFMWLEEN GIVTDMANFA  
<sup>51</sup> LSDPNAHRMR NFLANAPQAG SKSQRAKYGT AGYGVEARGP TPEEAQRE**KD**  
<sup>101</sup> **TRISK**KMETM GIYFATPEWV ALNGHRGPSP GQVKYWQNK R EIPDPNEDYL  
<sup>151</sup> DYVHAEKS**RL** ASEEQIL**RAA** TSIYGAPGQA EPPQAFIDEV AKVYEIN**HGR**  
<sup>201</sup> GPNQEOMKDL LLTAMEMKHR **NPRRALPKPK PKPNAPTQRP PGRLGRWIRT**  
<sup>251</sup> **VSD**EDLE

<b>VP3 PATCH 1</b>	<b>VP3 PATCH 2</b>	<b>VP3 Δ222-258</b>
<b>KRKK 99,102,105,106 DDDD</b>	<b>RRHR 159,168,198,200 DDDD</b>	

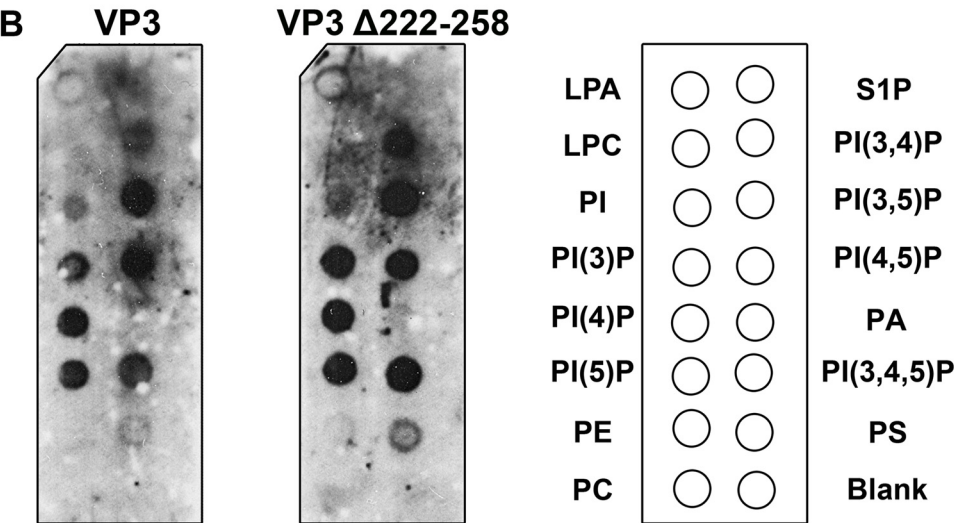


**FIG 3** The VP3 C-terminal domain is not required for binding to PPIs. (A) Amino acid sequence of VP3 from the IBDV Soroa strain (GenBank accession number [AAD30136.1](#)), where mutated residues are shown for PATCH 1 (bold and red), PATCH 2 (bold and blue), and the C-terminal domain missing in VP3Δ222–258 (bold and green). In a separate box, the residues numbers and the replacing of original K or R residues are shown. (B) Protein lipid overlay assay. Membranes spotted with 100 pmol of various lipids were incubated with 5 μg/ml of purified His-VP3 or His-VP3 short proteins. Bound proteins were detected using an anti-His mouse MAb, followed by incubation with goat anti-mouse Ig coupled to peroxidase and development with ECL. The right panel indicates the positions of spots corresponding to the different lipids. LPA, lysophosphatidic acid; LPC, lysophosphocholine; PI, phosphatidylinositol; PI(3)P, PI-3-phosphate; PI(4)P, PI-4-phosphate; PI(5)P, P-5-phosphate; PE, phosphatidylethanolamine; PC, phosphatidylcholine; S1P, sphingosine-1-phosphate; PI(3,4)P, PI-3,4-bisphosphate; PI(3,5)P, PI-3,5-bisphosphate; PI(4,5)P, PI-4,5-bisphosphate; PA, phosphatidic acid; PI(3,4,5)P, PI-3,4,5-trisphosphate; PS, phosphatidylserine. The images correspond to an experiment representing two independent trials.

with membrane lipids. For this, affinity-purified histidine-tagged VP3 protein (His-VP3), obtained as described in Materials and Methods, was incubated with lipid arrays containing biologically relevant lipids, all of them contributing to the relative predominance of anionic species in the inner leaflet of the plasma membrane, i.e., the cytosolic face of endosomes (53). As shown in Fig. 3B (left portion), the assay demonstrated a specific binding of His-VP3 polypeptide to the three monophosphate phosphoinositide (PPI) species, i.e., phosphatidylinositol-3-phosphate [PI(3)P], PI(4)P, and PI(5)P, to the three biposphate PPI species, PI(3,4)P<sub>2</sub>, PI(3,5)P<sub>2</sub>, and PI(4,5)P<sub>2</sub>, and to the triphosphate, PI(3,4,5)P<sub>3</sub>. Since the polybasic region is located in the C terminus of VP3, we hypothesized that this region of VP3 could be responsible for its interaction with negatively charged lipids present in the endosomal membrane. To test our hypothesis, we performed a lipid binding assay employing an affinity-purified histidine-tagged short version of VP3, a truncated version of the VP3 sequence encoding a polypeptide lacking the 36 C-terminal residues (His-VP3Δ222–258), constructed by the group of José F. Rodríguez (Madrid, Spain) to obtain the X-ray structure (23). As shown in Fig. 3B (middle portion), the truncated version of VP3 was able to specifically bind the set of lipidic species spotted in the array, strongly suggesting that the C-terminal region of

VP3 does not play a major role in its association with endosomal membranes. Taken together, these results indicate that VP3 associates with the cytosolic face of endosomes through its ability to bind PPIs, giving rise to specific structures resembling patches all along the endosomal membrane.

**Positively charged amino acids in the VP3 P2 domain mediate endosomal membrane association.** In order to better understand the mechanism underlying the association of VP3 with endosomal membranes, a mutagenic approach was followed employing two mutagenized versions of VP3. Four positively charged amino acids of the IBDV VP3 protein, predicted from the crystal structure, were replaced with negatively charged aspartic acid residues (PATCH 1 [P1] and PATCH 2 [P2]), as previously described (30) (Fig. 3A, PATCH 1 [bold and red] and PATCH 2 [bold and blue]). Mutant sequences were cloned in eukaryotic plasmid pcDNA and sequenced to confirm their identity, and the proteins were tested for endosomal membrane binding capacity.

We next utilized these constructs to assess the contribution of the P1 and P2 domains to the capacity of VP3 to associate with endosomes. First, we employed QM7 cells transiently overexpressing both EGFP-Rab5 wt and VP3 wt, P1 or P2, to evaluate the cellular distribution and colocalization of EGFP-Rab5 wt and mutated VP3-derived IFI signal. As shown in Fig. 4A, images and the quantitative colocalization analysis demonstrated the typical punctate distribution with a marked colocalization of both VP3 wt and P1 with EGFP-Rab5 wt. However, the P2-derived IFI signal depicted a cytosolic distribution of the protein. In addition, to further confirm the VP3 P2 cytosolic distribution, we used methanol permeabilization followed by paraformaldehyde (PFA) fixation of cells overexpressing EGFP-Rab5 wt and VP3 wt or P2. Confirming the efficacy of this method, the cells transfected with EGFP lost their characteristic cytosolic fluorescence, while EGFP-Rab5 wt-overexpressing cells preserved the punctate EGFP-Rab5 wt signal after methanol permeabilization prior to PFA fixation.

We next assessed cells overexpressing EGFP-Rab5 wt and VP3 wt or P2 by methanol permeabilization prior to PFA fixation. This resulted in the colocalization of EGFP-Rab5 wt green signal with VP3 wt IFI signal, which were unaffected by methanol permeabilization. On the other hand, methanol permeabilization caused the loss of characteristic VP3 P2-derived IFI signal (data not shown). Together, these results demonstrate the cytosolic localization of VP3 P2 and the requirement of P2 amino acids for endosomal membrane association of VP3.

In addition, we assessed the distribution of transiently overexpressing VP3 wt and the two mutants in QM7 cells transiently overexpressing EGFP-Rab5-Q79L. The expression of the constitutively active Rab5 mutant induces the formation of enlarged Rab5-positive vesicles, hence facilitating the visualization of endosome-associated proteins. As shown in Fig. 4B, and as expected, we observed a patchy distribution of both VP3 wt and P1 at the membrane of EGFP-Rab5-Q79L-positive vesicles. However, importantly, the specific IFI signal of P2 showed a cytosolic distribution. These results strongly suggest that positively charged amino acids in the P2 domain mediate VP3 association with endosomal membranes. We next sought to confirm if the VP3 P2 region mediates VP3 association with endosomes, by performing membrane fractionation of QM7 cells infected with IBDV or transiently overexpressing VP3 wt or VP3 P2. A previously described (55) method yielding a pellet of total cellular membranes and a supernatant representing the cytosolic fraction was employed, with minor modifications as described in Materials and Methods. We identified the membrane fraction with anti-E-cadherin antibodies and the cytosolic fraction by detecting glyceraldehyde-3-phosphate dehydrogenase (GAPDH), a glycolytic enzyme (56). As shown in Fig. 4C, the normalized ratios of membrane-bound VP3 to cytosolic VP3 from IBDV-infected or VP3 wt-overexpressing cells were 1 and 1.5, respectively, thus indicating that VP3 mostly occurs associated with cellular membranes. In contrast, VP3 P2-overexpressing cells show a drastic change in VP3 distribution, with an elevated accumulation of the protein within the cytosolic fraction (ratio of membrane-bound VP3 to cytosolic VP3, 0.4), reinforcing the notion that the P2 domain mediates VP3 association with endosomes.

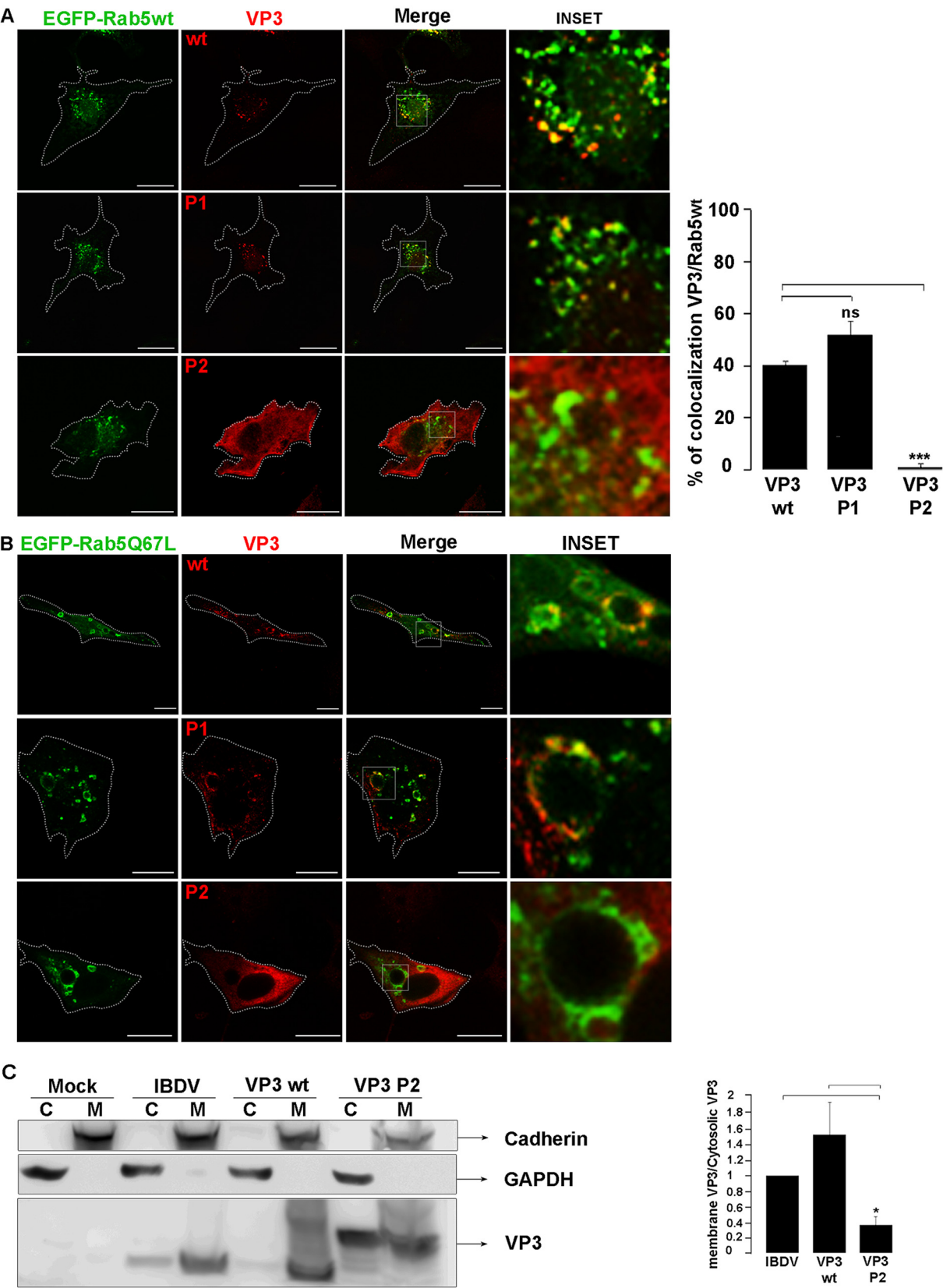


**FIG 4** The PATCH 2 domain mediates endosomal membrane association of VP3. (A) Analysis of the binding capacity of P1 and P2 versions of VP3 to endosomal membrane. QM7 cells were transiently cotransfected with EGFP-Rab5 wt and VP3 wt, P1, or P2 to evaluate their subcellular distribution and colocalization by indirect immunofluorescence analysis using anti-VP3 primary antibodies and Cy3-conjugated secondary (Continued on next page)

**Crucial role of VP3 P2 for IBDV replication.** We next sought to decipher the functional role of VP3 association with endosomal membranes in the context of the viral replication cycle. Noticeably, our first idea was to profit from the reverse genetic approach developed in the laboratory of J. F. Rodríguez and previously described (57) to generate P2-mutated viral progeny. To this end, a plasmid harboring a mutant version of segment A cDNA containing the P2 substitutions was constructed, but unfortunately, mutated viral progeny was not generated. Thus, we followed a different approach based on the observation of the crystallographic structure of VP3. Considering that crystallographic data demonstrated that VP3 is a dimer in solution and also in the crystal (23), we hypothesized that cytosolic VP3 P2 may bind IBDV-derived VP3, preventing the normal elapse of infection and acting as a dominant negative mutant polypeptide. To test this hypothesis, we constructed stable QM7-derived cell lines overexpressing EGFP, VP3 wt, VP3 P1, or VP3 P2. Transfected cells were grown as described in Materials and Methods and characterized by flow cytometry (fluorescence-activated cell sorting [FACS]) (Fig. 5A) and Western blotting (Fig. 5B). Both approaches demonstrated that the resulting cell lines express relatively similar high levels of the VP3 versions. Since we planned to utilize the aforementioned stable cell lines for performing quantitative titer determination and comparisons of virus infections, we verified that their growth rates present nonsignificant differences (Fig. 5C). Next we further characterized the stable cell lines by performing membrane fractionation of QM7 cells infected with IBDV or stably overexpressing VP3 wt or VP3 P2, as described before. Figure 5D shows that the normalized ratios of membrane-bound VP3 to cytosolic VP3 from QM7 cells that were IBDV infected or stably overexpressing VP3 wt were 1 and 1.05, respectively. Thus, similar to results shown in Fig. 4D, VP3 mostly was associated with cellular membranes. In contrast, QM7 cells stably overexpressing VP3 P2 showed a drastic change in VP3 distribution, with an elevated accumulation of the protein within the cytosolic fraction (ratio of membrane-bound VP3 to cytosolic VP3, 0.17). Next, we evaluated the subcellular distribution of EGFP- and VP3-derived IFI signal by LCSM and observed the expected typical punctuate perinuclear distribution for both forms VP3 wt and P1 and the cytosolic distribution of VP3 P2-derived IFI signal (Fig. 5E). Previously in our laboratory, based on the observed conspicuous effect of macropinocytic-specific disruptors in IBDV endocytosis, we demonstrated that a macropinocytic pathway is used as the major cellular mechanism for IBDV internalization, leading to a productive viral infection (10). Therefore, it was important to determine that the ectopic stable expression of the different versions of VP3 did not disturb the functionality of the macropinocytic pathway, which would be employed by the virus to infect those cell lines. To this end, we assessed the internalization of 10-kDa Alexa Fluor 488 conjugated dextran (Dx), a fluid-phase marker for macropinocytosis, by LCSM and FACS. We observed the same fluorescence intensity in the three cell lines, indicating nonsignificant differences in their ability for performing functional macropinocytic uptake of dextran (Fig. 5F and G). Together, our results indicate that these cell lines are suitable for the assessment of our hypothesis. Thus, QM7 cells stably overexpressing

#### FIG 4 Legend (Continued)

antibodies to detect VP3-derived signal. The insets show colocalization areas of VP3, P1, or P2 with Rab5-positive vesicles (EGFP-derived signal). The colocalization analysis was performed employing ImageJ software, and results are represented in the bar graph. Thirty cells per condition were scored for each experiment. The images correspond to an experiment representing three independent trials. Scale bars represent 10  $\mu$ m. \*\*\*,  $P < 0.01$ . (B) Analysis of the binding morphology of VP3 P1 and P2 mutants with endosomes. QM7 cells were cotransfected with EGFP-Rab5-Q79L and VP3 wt, P1, or P2 and the subcellular distribution pattern were analyzed by indirect immunofluorescence employing anti-VP3 primary antibodies and Cy3-conjugated secondary antibodies to detect VP3. The insets show an enlarged area displaying the distribution patterns of VP3, P1, or P2 to the membrane of Rab5-Q79L endosomes. The images correspond to an experiment representing three independent trials. Scale bars represent 10  $\mu$ m. (C) Analysis of VP3 wt or P2 protein localization. QM7 cells were transiently transfected with VP3 wt or P2 or infected with IBDV at an MOI of 1 PFU/cell, and the monolayers were processed for subcellular fractionation at 24 h p.i. following a protocol described in Materials and Methods. Briefly, a pellet of total cellular membranes and a supernatant representing the cytosolic fractions were obtained and analyzed by Western blotting. Primary anti-VP3 antibodies were used to detect VP3 wt or P2 protein. We used anti-E-cadherin primary antibody to identify the membrane fraction and primary antibodies anti-glyceraldehyde-3-phosphate dehydrogenase (anti-GAPDH) to monitor the cytosolic fraction. Corresponding HRP-conjugated anti-mouse and anti-rabbit secondary antibodies were used to detect immunoreactive bands by chemiluminescence. The Western blot image and the data shown in the normalized bar graph correspond to an experiment representing three independent trials. \*,  $P < 0.1$ . Error bars show SD.

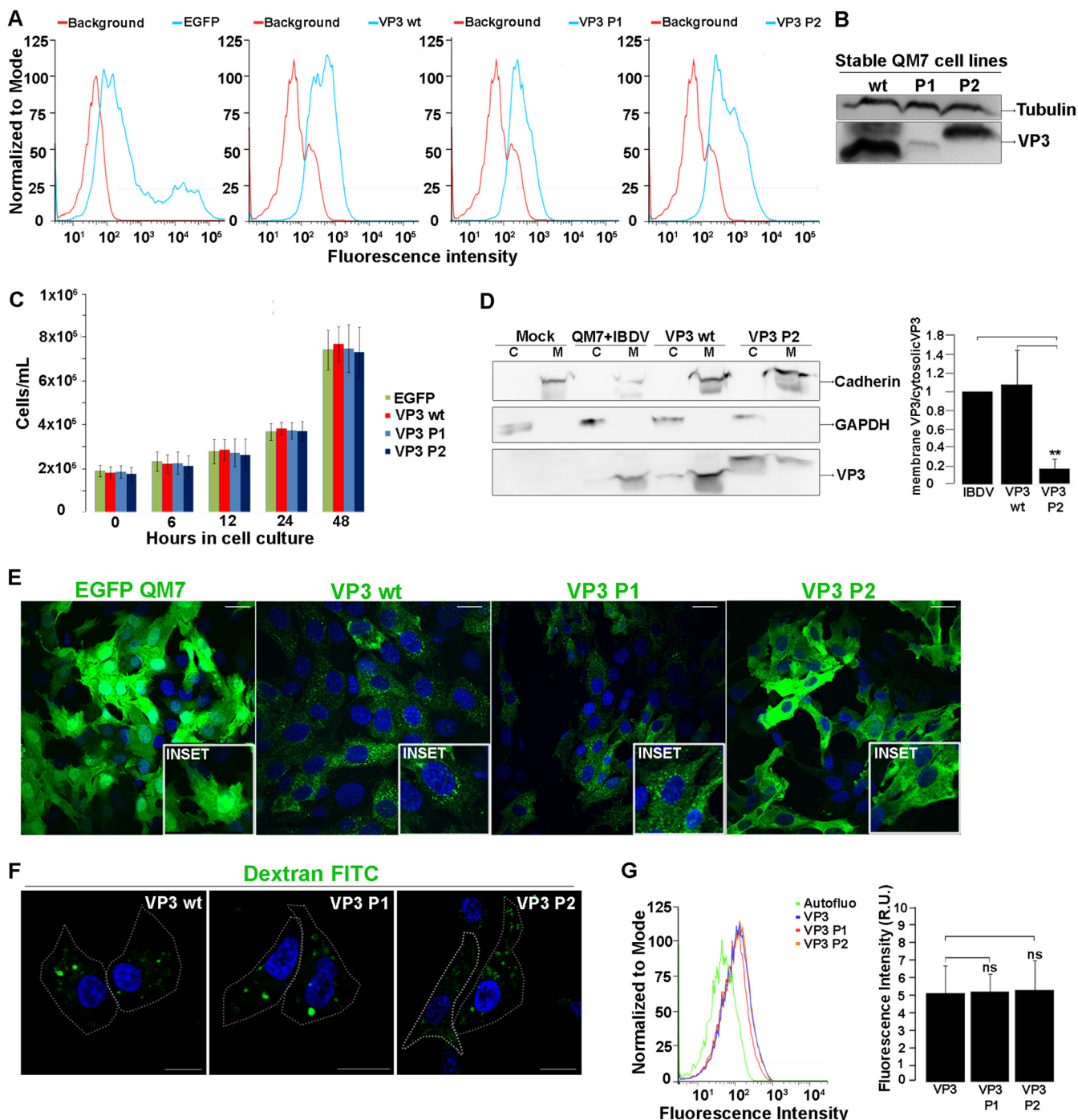


**FIG 5** Characterization of stably overexpressing QM7-derived cell lines. (A) VP3 expression level analysis. The cell lines stably expressing EGFP, VP3, P1, and P2 were generated by a batch cell selection procedure and processed by flow cytometry (FACS) as described in Materials and Methods. Representative FACS histograms from three independent trials show the fluorescence intensity in relative units, for each cell line. (B) VP3 expression level analysis. The expression of VP3 in cell lines stably expressing VP3, P1, and P2 was analyzed by Western blotting as described in Materials and Methods. Corresponding HRP-conjugated anti-mouse and anti-rabbit secondary antibodies were used to detect immunoreactive bands by chemiluminescence. The Western blot image corresponds to an experiment representing three independent trials. (C) Growth rates of stable cell lines. Cell lines were grown in selective culture medium, and the cells were harvested and counted with a Neubauer chamber at 0, 6, 12, 24, and 48 h postplating as described in Materials and Methods. The bar graph showing the number of cells at each time point in cell culture corresponds to an experiment representing five independent trials. Error bars show SD. (D) VP3 wt or P2 protein localization analysis in stable cell lines. QM7 cells stably overexpressing VP3 wt or P2 or infected with IBDV Soroa at an MOI of 1 PFU/cell or mock infected were harvested at 24 h p.i. Following a protocol described in Materials and Methods, the monolayers were processed for subcellular fractionation and analyzed as for Fig. 4C. The Western blot image and the data shown in the normalized bar graph correspond to an experiment representing three independent trials. Error bars show SD. \*\*,  $P < 0.05$ . (E) Subcellular distribution of stably overexpressing QM7-derived cell lines. EGFP, VP3, P1, and P2 proteins from the stable cell lines were characterized by indirect immunofluorescence employing primary antibodies to detect VP3-derived signal or the specific green signal of EGFP by CLSM. Insets show the typical perinuclear punctate distribution for both VP3 wt and P1 and the cytosolic distribution of EGFP and P2. The images correspond to an

(Continued on next page)

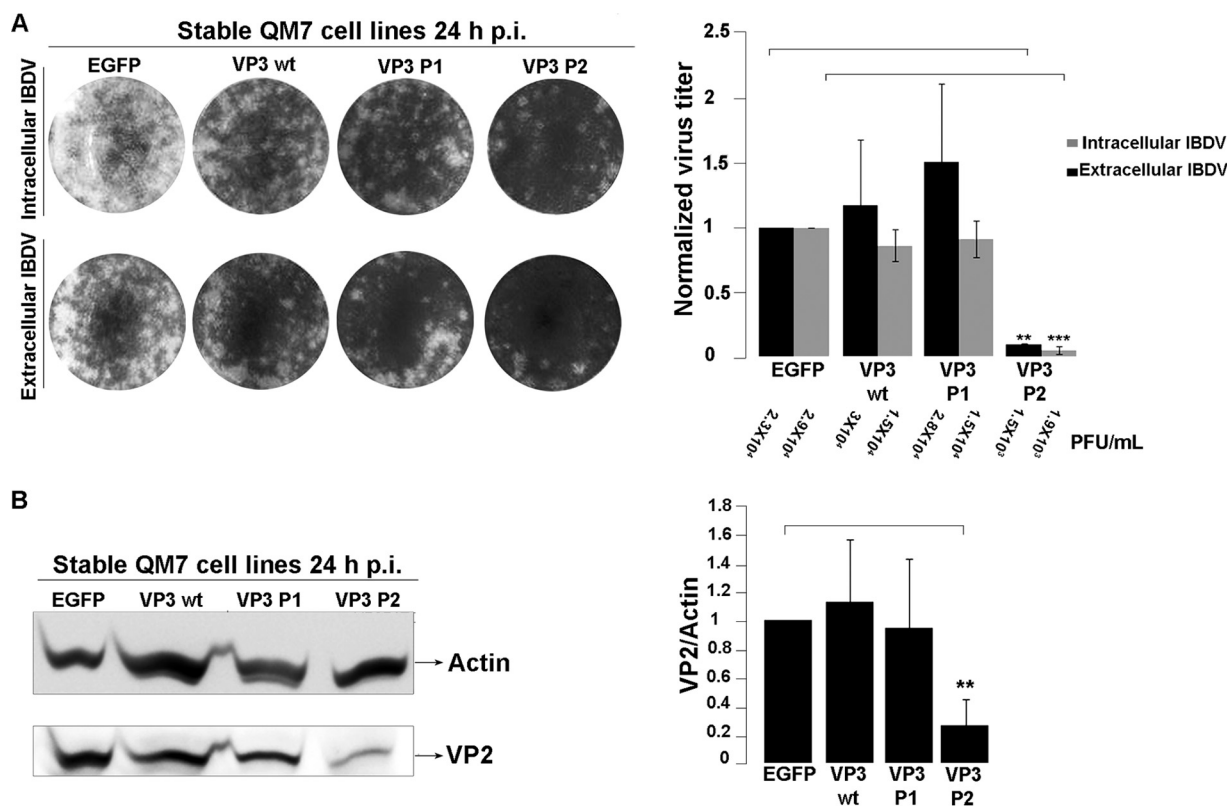


**FIG 6** VP3 P2 dominant negative effect in the IBDV replication cycle. (A) Impact of VP3 P2 expression in IBDV progeny. QM7-derived cell lines stably overexpressing EGFP, VP3 wt, VP3 P1, or P2 were infected with IBDV Soroa at an MOI of 1 PFU/cell, the supernatants were collected to perform extracellular virus titration, and cellular pellets were processed for intracellular virus titration at 24 h p.i. as described in Materials and Methods. On the left, the wells of intra- and extracellular virus titrations at a 1/100 dilution, corresponding to the infections of QM7 cells stably expressing EGFP, VP3 wt, P1, or P2, are shown. Results from a representative experiment from four independent trials are shown and represented in the normalized bar graph. Error bars show SD. \*\*,  $P < 0.05$ ; \*\*\*,  $P < 0.001$ . The crude viral titers are shown below the bar graphs. (B) VP2 intracellular accumulation analysis in stable cell lines. QM7-derived cell lines stably overexpressing EGFP, VP3 wt, P1, or P2 were infected with IBDV Soroa at an MOI of 1 PFU/cell, and the relative amounts of VP2 were analyzed by Western blotting at 24 h p.i. as described in Materials and Methods. Corresponding HRP-conjugated anti-mouse and anti-rabbit secondary antibodies were used to detect immunoreactive bands by chemiluminescence. The Western blot image and the data shown in the normalized bar graph correspond to an experiment representing three independent trials. Error bars show SD. \*\*,  $P < 0.05$ .

EGFP, VP3 wt, VP3 P1, or VP3 P2 were infected with IBDV at an MOI of 1 PFU/cell, and at 24 h p.i., the cells were processed for intra- and extracellular virus titration and VP2 intracellular accumulation by Western blotting. As shown in Fig. 6A, there was a significant decrease in viral production in VP3 P2-expressing cells compared with that in cells expressing EGFP, VP3 wt, or VP3 P1, which did not affect the production of an infective viral progeny. Accordingly, we observed a significant decrease in VP2 accumulation in VP3 P2-expressing cells (Fig. 6B). These results further confirm our hypothesis and demonstrate the relevance of the association of VP3 to endosomes for the success of the IBDV replication cycle. Importantly, this association relies on the P2 positively charged structural domain of VP3.

## DISCUSSION

Regardless the nature of the cell surface receptor used and the endocytic pathway employed for cell internalization, nonenveloped viruses are delivered to early endo-

### FIG 5 Legend (Continued)

experiment representing three independent trials. Scale bars represent 10  $\mu$ m. (F and G) Macropinocytic pathway functionality of stably overexpressing QM7-derived cell lines. The stable cell lines were incubated with the macropinocytic substrate 10-kDa Alexa Fluor 488-dextran for 1 h and processed for analysis by CLSM and flow cytometry (FACS) as described in Materials and Methods. CLSM images correspond to an experiment representing three independent trials. Scale bars represent 10  $\mu$ m. A representative FACS histogram of three independent trials shows the fluorescence intensity in relative units, also presented in a bar graph. Error bars show SD. FITC, fluorescein isothiocyanate.

somes (EEs), characterized by the presence of the GTPase Rab5 protein and early endosome antigen 1 (EEA1) (58, 59). Some viral agents delay their cytosol penetration and trafficking from EEs to late endosomes (LEs), characteristically enriched in GTPase Rab7 (60). Of the various small GTPases present in endosomes, Rab5 and Rab7 are the most critical for the function of EEs and LEs, respectively (61). Thus, subsequent virus uncoating and cytoplasm invasion occur either from EEs (early-penetrating viruses [E-PVs]) or from LEs (late-penetrating viruses [L-PVs]). In a recent report (10), we have shown that following macropinocytic internalization, IBDV particles reached the EEs and a functional GTPase Rab5-regulated endocytic pathway was required for virus replication. However, GTPase Rab7 does not seem to be required, as overexpression of a dominant negative form of this protein did not impair viral internalization. This finding is in good agreement with our previous study showing that IBDV replication complexes locate in endosomal structures, showing features of early and intermediate endosomes but lacking Rab7 and degradative activity (10, 11). In this study, we demonstrated that IBDV uncoating occurs in EEs and that subsequently a bifurcated pathway is followed by the capsid protein VP2 and the RNPs. Thus, the internalized virus-derived VP2 proteins traffic in the pathway of lysosomal degradation and the RNPs extrude from the incoming-vesicle to encounter naive endosomes for association and viral replication to commence (Fig. 1). So first, our findings allowed us to localize IBDV, a distinct dsRNA virus belonging to the *Birnaviridae* family, in the list of E-PVs. EEs constitute a heterogeneous collection of organelles involved in molecular sorting and recycling of plasma membrane components. The luminal pH is in the range of 6.5 to 6.0, which allows the activation of E-PVs such as vesicular stomatitis virus or the simian rotavirus strains RRV and SA11-4S (60, 62). It is well known that the *in vitro* stability of IBDV particles depends on the presence of calcium. If calcium is removed from the medium by chelation, the outer layer disassembles (18, 63). Thus, it is tempting to hypothesize that the drop in luminal calcium concentration in the endosomal compartment may trigger virus uncoating, yielding RNPs that reach the cytoplasm through a disrupted vesicle membrane. However, we cannot rule out the possibility of a more complex scenario with a combination of factors needed for triggering IBDV disassembly. We have integrated current and previous observations to elaborate a schematic model of IBDV receptor recognition, internalization, and establishment of endosome-associated viral replication niche inside the infected cells, depicted in Fig. 7.

Our data further support those from previous studies showing VP3-mediated association of viral RNPs with endosomal membrane (11). Indeed, we aimed to identify the endosomal membrane partner(s) responsible for engaging VP3 in infected cells. So we undertook careful scanning for motifs in the VP3 sequence potentially involved in known protein-protein interactions, but we failed to find any. Instead, we observed several positively charged amino acid clusters spread overall the protein sequence, and therefore, the role of cellular lipids in the engagement of VP3 was analyzed (Fig. 3A). Indeed, electrostatic interactions between anionic lipids and surface-exposed polycationic protein domains play a key role on the targeting of many proteins to cellular membranes (53). We observed a clear capacity for binding of VP3 to phosphoinositides (PPIs), a term used to describe the seven types of phosphorylated phosphatidylinositols (Fig. 3B). PPIs are pivotal membrane lipid components that help define membrane identity and coordinate a plethora of signaling pathways and interactions at the membrane-cytosol interface (64). This makes them prime targets for pathogens to harness for creating their environments. Thus, our observation was not surprising given that (i) it is known that both bacteria and viruses exploit PPIs to remodel host cell compartments for establishing effective replication platforms and (ii) PPIs, even though they make up a small fraction of total cellular phospholipids (65), are specific constituents of the cytosolic leaflet of plasmatic and early endocytic vesicle membranes. So our observation is in complete agreement with the E-PV feature of IBDV. These PPI species can be segregated into microdomains when bound by polycationic protein regions, increasing their local accumulation and generating an electric field capable of strongly binding cationic proteins, peptides, and ions (66, 67). This could be the

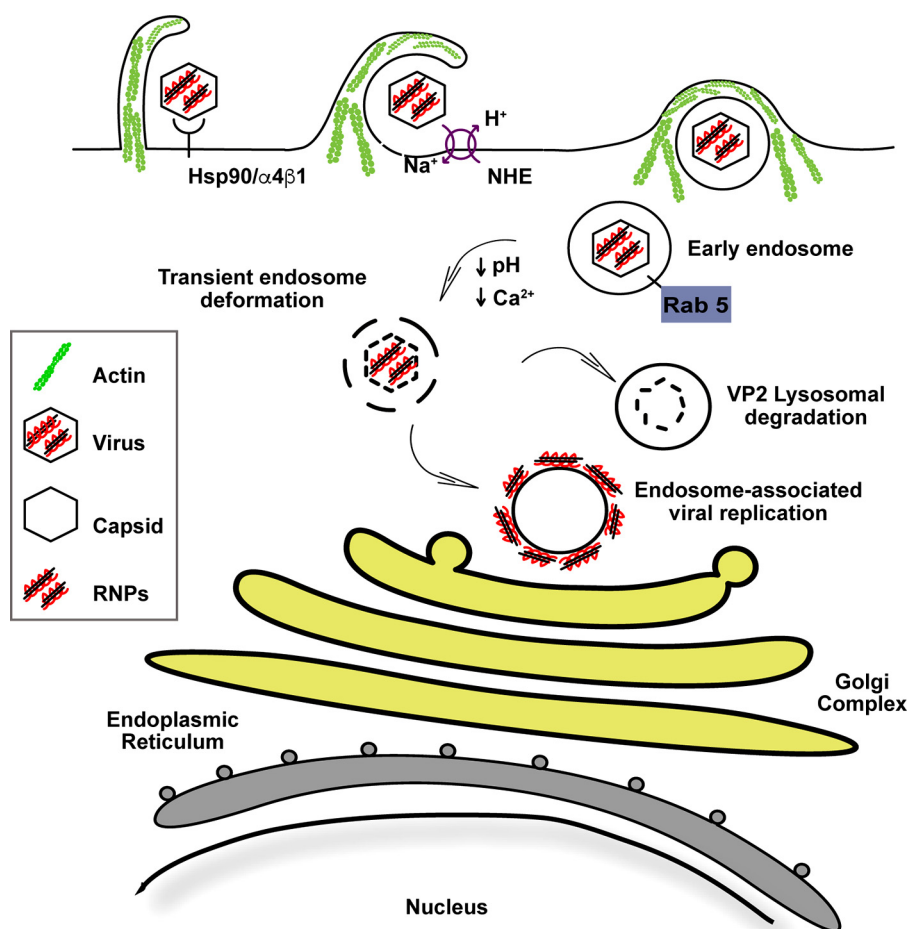


**FIG 7** Schematic model for IBDV internalization and establishment of the endosome-associated replication niche. Employing the cellular receptor complex composed by Hsp90 and  $\alpha 4\beta 1$  integrin (72, 80), IBDV particles hijack the macropinocytic pathway from the host cells to be internalized (9) and then traffic to early endocytic structures in a Rab5-dependent manner. There the particles profit from the endosomal acidification and the subsequent low  $\text{Ca}^{2+}$  concentration to promote the uncoating of viral capsid and the exposure of one of the capsid-associated peptides, PEP46, which is able to deform biological membranes, leading to the formation of pores on the endosomal membrane (16). Our proposed model shows that after internalization, while disassembled viral capsids of IBDV internalized particles reach late endocytic compartments for degradation, IBDV RNPs would be extruded from the pierced endosomes and associate with membrane phosphoinositides on the cytosolic face of naive early endosomes, through the VP3 PATCH 2 region, assembling patches all along the endosome membrane. Afterwards, the RNPs, associated with the endosomal compartments, traffic along the microtubules to reach the perinuclear region, establishing physical contact with the Golgi complex, where the viral replication occurs (11).

required scenario for giving rise to VP3-induced endosome-associated structures, resembling “patches” when observed by CLSM, where viral replication occurs. Of course, we cannot rule out the possibility that an additional interaction mediated by an endosomal protein is involved in the binding of VP3 to the membrane endosomes.

While identifying positively charged amino acid residues within VP3 sequence, we first observed the predominance of lysines (K) and arginines (R) within the C terminus of the polypeptide, which were especially attractive but failed to be the sites for engagement with the endosomal membranes. Structural predictions indicated that the C terminal domain of the polypeptide lacks a fixed three-dimensional structure, defined by secondary-structure elements in a given packing, but it is mainly unstructured and mobile (23). Moreover, since the VP3 C-terminal domain harbors several others functions within the viral replication cycle (27), it was not unexpected to find that the VP3 sequence encoding a polypeptide lacking the 36 C-terminal residues (His-VP3 $\Delta$ 222–258) was not involved in engaging endosomal membranes. Instead, we found that VP3

binds to endosomes through a structured domain (P2). A variety of membrane-associated proteins have PPI-binding domains with binding pockets for particular phospholipids. These domains recognize phosphoinositides with structural specificity, but none of those structural traits are present in VP3 polypeptide (68, 69). The membrane curvature formation may also be triggered by just the assembly of proteins on the membrane, without specific membrane binding properties. This mechanism is recently proposed as protein “crowding” for curvature formation (70, 71). In this case, the assembly of proteins on the membrane with some anchoring to the membrane can bend the membrane. The protein assembly of adaptor protein complex at the clathrin-coated pit might be considered to be such an example (70). Indeed, we speculate the capacity of VP3 to produce a deformation in the endosomal membrane to give rise to specific “replication niches,” which could be spherule-like structures connected to the cytoplasm but with the capacity to keep the replication machinery hidden from innate immunology components present in the cytoplasm.

As mentioned above, we aimed to test the functional role of VP3 association with endosomal membranes in the context of the viral replication cycle by profiting from a reverse genetic approach developed by Rodríguez Aguirre’s laboratory to generate P2-mutated viral progeny (72). Using this approach, P1 and P2 mutations were introduced in the reverse genetic system, but unfortunately, infective viral progeny was not generated. We reasoned that this could be the consequence of two different phenomena. First, P2 amino acid substitution could hamper the correct protein folding and consequently the whole viral particle would not be assembled inside the transfected cell. However, we discarded this possibility by virtue of the experimental observations made by Valli and collaborators (30), which showed that none of the multiple substitutions of positively charged amino acids affected the capacity of IBDV VP3 to form dimers, suggesting that these mutations do not produce a drastic disturbance of the overall structure of the protein. The second possibility we contemplated was that the replication of the mutated viral particles was not efficient enough to allow for its detection and evaluation of the functional role of VP3 P2 in the context of viral infection. Certainly, our approach to investigate this point, based on the hypothesis that VP3 P2 acts as a dominant negative factor recruiting VP3 through the formation of VP3 P2-VP3 dimers sequestering VP3 and hampering the normal infection course inside the stably VP3 P2-expressing QM7 cell line, provided indirect evidence of the role of VP3 endosome association. Indeed, studies aimed to define structural features of the VP3 endosomal membrane-associated compartments and its role in viral replication are ongoing, and we hope they will shed light on this and other aspects of IBDV replication.

**Evolutionary intermediaries between +ssRNA and dsRNA viruses.** Viruses are exceptionally diverse in structure, genetic organization, and replication strategies. Birnaviruses display unique features among dsRNA viruses, which tightly link them to +ssRNA viruses, such as nodaviruses and alphatetraviruses, robustly arguing for their role as evolutionary intermediaries between +ssRNA and dsRNA viruses, with the first evidence regarding birnavirus polymerase obtained back in 1988 (73). The RdRp of two +ssRNA viruses (*Thoseaasigna virus* [TaV] and *Euprosternaelaeasavirus* [EeV]) formerly related to the tetraviruses and recently grouped in a separate family, the *Permutotetraviridae* (T=4) (74), shares with the birnavirus VP1 a unique polymerase motif rearrangement: their catalytic motifs are arranged in the permuted order C-B-A in the primary sequence of the palm domain, in contrast to the canonical A-B-C order found in all other viruses and organisms (27, 75, 76). However, since TaV and EeV possess the conserved -GDD- sequence in motif C, and birnavirus VP1 has an altered version (-ADN-), it is likely that birnaviruses originated from a TaV/EeV-like ancestor in which the polymerase permutation had already taken place. Regarding the capsid, birnavirus coat protein contains domains homologous to the coat proteins of both +ssRNA and dsRNA viruses. In an elegant study, Johnson et al. (77) showed that a number of characteristics position birnavirus VP2 as an intermediate between the outer shell proteins of the dsRNA T=13 *Reoviridae* and those of the positive-strand +ssRNA T=3 nodaviruses and

T=4 tetravirus. The bisegmented nature of birnaviruses genome, with one segment encoding the capsid protein and the second the RdRp, is also retrieved in nodaviruses and in some alphatetraviruses, with the former undergoing catalytic maturation to give rise to membrane-active peptides (PEP46 and  $\gamma$ , respectively), as mentioned above. Finally, the birnavirus VPg-linked genome replication strategy is an additional common feature bringing birnaviruses and some other +ssRNA viruses together. Here we present evidence supporting the evolutionary intermediary position for birnavirus by providing original data regarding the replication strategy of a prototype member of *Birnaviridae* family, IBDV. We show that replication of IBDV hijacks cell-derived endosomal membranes for replication into host cells. Our results constitute the first direct experimental evidence showing that a membranous compartment, such as endosomes, is required by a dsRNA virus to replicate. We show that VP3 polypeptide associates with the endosomal membranes with a punctate distribution pattern, resembling patches all along the vesicle membrane, and is responsible for the association of viral replication complexes with PPIs into the cytosolic side of endosomes. We identified the positively charged amino acid structural domain of VP3 involved in this association (P2) and determined its key functional role in the context of the virus life cycle. Indeed, we hypothesize that VP3 is able to give rise to membranous structures (such as pockets or spherules) hiding dsRNA molecules from the vast number of cellular sentinels where RNA replication occurs. In a recent elegant study, Ertel et al. (78) reported a detailed study of Flock House virus RNA replication compartments (spherules) by cryo-electron tomography (cryo-ET), whose substantial advantages include rapid cryofixation of samples in a much more native state and direct imaging of intrinsic electron density. They show the resulting spherule structures revealing filamentous internal RNA templates, a multimeric protein crown gating the necked aperture to the cytoplasm, associated cytoplasmic filaments likely representing nascent RNAs, and strong correlation between RNA template length and spherule size. In order to advance understanding of the crucial relationship between birnaviruses and the intracellular membranes on which they replicate their RNA genomes, we aim to combine three-dimensional (3D) ultrastructural imaging after cryo-ET with quantitative biochemical data to model the architecture and organization of IBDV RNA replication complex, which is completely unknown to date. Finally, with the aim of further understanding the evolutionary history of dsRNA viruses, it will be extremely interesting to reveal possible VP3 structural and functional parallelism to *Reoviridae* T=2 core proteins.

## MATERIALS AND METHODS

**Cell lines and virus.** QM7 (quail muscle myoblasts; ATCC number CRL-1962) and HeLa (human epithelial cervical cancer cells, ATCC number CCL-2) cells were grown in Dulbecco's modified Eagle's medium (DMEM; number 12-800058; Life Technologies, Argentina) supplemented with penicillin-streptomycin (10,000 U/ml; number 15140122; Life Technologies) containing 10% fetal bovine serum (Gibco FBS, qualified, South American origin, number 10270-106; Life Technologies) at 37°C in an atmosphere of 95% air and 5% CO<sub>2</sub>.

The IBDV Soroa strain, a virulent serotype 1 virus, was propagated in QM7 cells as previously described (28). For virus stock production, QM7 cells were grown until 70% confluence and infected with IBDV Soroa at a multiplicity of infection (MOI) of 0.05 PFU/cell. When cytopathic effect was complete (72 to 96 h postinfection [p.i.]), the cells and the supernatant were collected, supplemented with 20% polyethylene glycol 8000 and 3 M NaCl, and incubated for 12 h at 4°C. The virus was pelleted at 800 × g for 30 min, and the resulting pellet was resuspended in PES buffer [25 mM piperazine-*N,N'*-bis(2-ethanesulfonic acid) (pH 6.2), 150 mM NaCl, and 20 mM CaCl<sub>2</sub>].

**Antibodies and reagents.** Western blot and confocal laser scanning microscopy (CLSM) analyses were carried out using the following primary antibodies: rabbit anti-VP3- and rabbit anti-VP2-specific sera as previously described (79). Mouse anti-GM130 antibodies were obtained from BD Biosciences (number 610822; Becton Dickinson, Argentina), and mouse anti-PDI monoclonal antibodies (MAbs) (Abcam; number ab2792) were kindly provided by Javier Magadán (IHEM, CONICET, Universidad Nacional de Cuyo, Mendoza, Argentina); mouse anti-pan-cadherin (number C1821), anti- $\beta$ -tubulin (number T5201), and anti-actin (number A5441) monoclonal antibodies were purchased from Sigma-Aldrich (Buenos Aires, Argentina). Mouse anti-GAPDH (number A01622) monoclonal antibodies were purchased from GenScript (USA). Secondary goat anti-rabbit antibodies conjugated with Alexa Fluor 488 (number A21206) and Hoechst 33342 (number H1399) were purchased from Molecular Probes (Thermo Fisher, Buenos Aires, Argentina). Donkey anti-rabbit antibodies conjugated with Cy3 (number 711-165-152) and donkey anti-mouse antibodies conjugated with Cy3 (number 715-165-150) were purchased from Jackson

ImmunoResearch (USA). Horseradish peroxidase (HRP)-conjugated anti-rabbit and anti-mouse secondary antibodies (number A0545 and A9044, respectively), mouse anti-His antibody (number H1029), and goat-anti mouse Ig conjugated to peroxidase (number A4416) were purchased from Sigma-Aldrich (Buenos Aires, Argentina). Alexa Fluor 488-conjugated 10,000-molecular-weight (MW) dextran (Dx; number D22910; 1 mg/ml) was purchased from Molecular Probes (Thermo Fisher, Buenos Aires, Argentina). Digitonin was a gift from Néstor Guerrero from the Centre de Physiopathologie, Toulouse, France. Bafilomycin A1 (BafA1; number B1793) was purchased from Millipore Sigma (Ontario, Canada).

**Plasmids and transfections.** Plasmids encoding EGFP-Rab7 wt and EGFP-Rab7-Q67L were kindly provided by Bo van Deurs (University of Copenhagen, Copenhagen, Denmark), and plasmids encoding EGFP-Rab5 wt and EGFP-Rab5-Q79L were kindly provided by Philip D. Stahl (Washington University, St. Louis, MO). Plasmids pcDNAVP3wt, pcDNAVP3Patch 1, and pcDNAVP3Patch 2 were constructed by Valli and collaborators for a previous study (30) and kindly provided by José F. Rodríguez (Madrid, Spain) to our group. For transient transfections, plasmids were transfected in 80% confluent cell monolayers employing Lipofectamine 3000 (number L300015; Invitrogen, Thermo Fisher, Buenos Aires, Argentina) following the manufacturer's recommendations, and after 12 h, cells were fixed with 4% paraformaldehyde (PFA) or infected with IBDV with a specific MOI and processed according to the experimental scheme.

**Sequence analysis.** DNA of pcDNAVP3wt, pcDNAVP3Patch 1, and pcDNAVP3Patch 2 constructions was purified using a QIAprep Spin Miniprep kit (Qiagen GmbH, Germany) and sequenced by the nucleotide sequencing service of Macrogen, South Korea. Alignments and prediction of amino acid sequences were performed using the Aliner and Translator tools from the JustBio website (<http://www.justbio.com>).

**His-VP3 wt and His-VP3 short protein expression and purification.** Plasmid constructions bearing the histidine-tagged wild type and the short version of VP3, a truncated version of the VP3 sequence encoding a polypeptide lacking the 36 C-terminal residues (His-VP3 $\Delta$ 222–258), were constructed by the group of José F. Rodríguez to obtain the X-ray structure (23). Procedures to express recombinant His-tagged VP3s in insect cells by using recombinant baculovirus as well as to purify the polypeptides by metal affinity chromatography were previously described (24).

**Lipid overlay assay.** Membrane lipid strips (number P-6002) spotted with 100 pmol of phospholipids, including phosphatidylinositol (PI) and its seven phosphorylated derivatives (phosphoinositides [PPIs]), lysophosphatidic acid (LPA), lysophosphocholine (LPC), phosphatidylethanolamine (PE), phosphatidylcholine (PC), sphingosine-1-phosphate (S1P), phosphatidic acid (PA), and phosphatidylserine (PS) were purchased from Echelon Biosciences (USA). Membranes were blocked for 90 min at room temperature (RT) in blocking buffer (BBF; phosphate-buffered saline [PBS] supplemented with 5% lipid-free bovine serum albumin [BSA], 0.1% Tween 20, 3 mM CaCl<sub>2</sub>) and then incubated for 90 min with 5  $\mu$ g/ml of purified His-VP3 or His-VP3 short proteins diluted in BBF. Membranes were washed with BBF and then incubated for 1 h with an anti-His mouse MAb, followed by incubation with goat-anti mouse Ig coupled to peroxidase. Finally, after washing with BBF, ECL was used to detect bound proteins. These experiments were performed at José F. Rodríguez's laboratory (Madrid, Spain).

**Selective permeabilization and indirect immunofluorescence assay.** HeLa cells were grown on coverslips in an M24 multiwell plate for 12 h to approximately 70% confluence and infected with IBDV Soroa at an MOI of 1 PFU/cell. After 24 h p.i., the cells were fixed with 4% PFA for 15 min at RT, washed with 1 $\times$  PBS (pH 7.4), and permeabilized with 0.05% saponin in PBS containing 0.2% defined BSA at RT or selectively permeabilized with cold digitonin (5  $\mu$ g/ml) in 1 $\times$  PBS, on ice, for 5 min and then extensively washed with cold 1 $\times$  PBS. Then the cells were incubated with anti-VP3, anti-PDI, or anti-GM130 primary antibodies overnight (ON) at 4°C in a humidity chamber, and after extensive washing, cells were incubated with secondary antibodies conjugated with Alexa Fluor 488 or Cy3 for 1 h 30 min, followed by extensive washes in 1 $\times$  PBS. The coverslips were mounted in Mowiol, analyzed by CLSM employing a Nikon C1 confocal microscope system and EZ-C1 software (Nikon, Japan), and processed using Adobe CS5 (Adobe Systems).

**Membrane fractionation in transient and stably transfected avian cells.** QM7 cells transiently or stably transfected with VP3 wt or VP3 PATCH2 (P2) were grown in T75 flasks, or QM7 cells were grown in T75 flasks and then infected with IBDV Soroa at an MOI of 1 PFU/cell and harvested in 600  $\mu$ l of ice-cold homogenization buffer (25 mM HEPES, 100 mM NaCl, 1 mM EDTA [pH 7.4], and protease inhibitor cocktail) at 4°C 24 h p.i. After centrifugation at 68  $\times$  g and 4°C for 10 min to remove cellular debris, the supernatants were collected and ultracentrifuged at 100,000  $\times$  g and 4°C for 1 h to yield a pellet of total cellular membranes and a supernatant representing the cytosolic fraction. The membrane pellets were dissolved in homogenization buffer (25 mM HEPES [pH 7], 100 mM NaCl, 5 mM MgCl<sub>2</sub>, 1% Triton X-100, 10% glycerol, 1 mM dithiothreitol [DTT], and protease inhibitor) by incubation at 4°C for 15 min. The entire membrane fraction and 20% of the cytosolic fraction were mixed with 4 $\times$  Laemmli buffer to a final concentration of 1 $\times$  and subjected to SDS-PAGE and immunoblot analysis.

**Generation of stable cell lines.** QM7 cells were plated at a density of 125/well on a 24-well plate, grown in cell culture medium for 12 h, and then transfected with 0.5  $\mu$ g of EGFP, pcDNAVP3wt, pcDNAVP3Patch 1 (P1), or pcDNAVP3Patch 2 (P2) using Lipofectamine 3000 (number L300015; Invitrogen, Thermo Fisher, Buenos Aires, Argentina) following the manufacturer's recommendations. After 12 h, cell culture medium was removed, cells washed twice with 1 $\times$  PBS, and added at 1 ml per well of selection medium containing 1 $\times$  DMEM, 10% FBS, and 1 mg/ml of G418 (number ant-gn-5; InvivoGen, USA) without penicillin-streptomycin. The selection medium was replaced every 3 days during a 21-day period, and cells were expanded according to the growth rate. Finally, the stable cell lines were

characterized by immunofluorescence, flow cytometry (FACS), and Western blot analysis to determine the relative amounts of proteins and the homogeneity of each population.

**Cytosolic protein extraction by methanol permeabilization.** QM7 cells grown on coverslips in 24-well plates were transfected with EGFP, EGFP-Rab5 wt, VP3 wt, P1, or P2 employing Lipofectamine 3000. After 12 h, transfected cells were methanol permeabilized at  $-20^{\circ}\text{C}$  for 90 s to extract cytosolic proteins or left in rich medium. Then the cells were fixed with 4% PFA at RT for 15 min. After extensively washing with PBS, cells were permeabilized with 0.05% saponin in PBS containing 0.2% BSA at RT for 20 min. Finally, cells were mounted in Mowiol or incubated with anti-VP3 primary antibodies for 1 h 30 min at RT in a humidity chamber, and after extensive washing, the cells were incubated with secondary antibodies conjugated with Cy3 for 1 h 30 min, followed by extensive washes in PBS. Then the coverslips were mounted with Mowiol and analyzed by CLSM. Images were captured using a Nikon C1 confocal microscope system and the EZ-C1 program (Nikon, Japan) and processed using Adobe CS5 (Adobe Systems).

**Virus titration by plaque assay.** QM7 cells were grown in 24-well culture plates to 70% confluence and infected with serial dilutions of IBDV. After virus adsorption, monolayers were covered with a mixture of 1:1 2 $\times$  DMEM and 1.4% low-melting-point agarose and maintained for 5 days at  $37^{\circ}\text{C}$ . The cellular monolayers were fixed with 10% Formol, the semisolid medium was carefully removed, and the monolayers were stained with 1% crystal violet in order to readily identify plaques, which were counted to determine the titer of viral samples in terms of PFU per milliliter. To titrate intracellular infective viral particles, infected cells were collected with 1 ml of DMEM, subjected to three freeze-thaw cycles, and then centrifuged to eliminate cellular detritus. The supernatants corresponding to a viral suspension were employed for titration. To titrate extracellular infective viral particles, the supernatants of infected cells were collected.

**Macropinocytosis functionality assay.** Cell lines stably expressing VP3 wt, P1, or P2 were grown on coverslips in 24-well plates. After 12 h of plating, cells were incubated for 60 min with 1 mg/ml of 10-kDa Dx-Alexa Fluor 488 in serum-free DMEM. Finally, the cells were washed three times with PBS, fixed with 4% PFA at RT for 15 min, mounted in Mowiol plus Hoechst, and analyzed by CLSM. For FACS assays, cell lines stably expressing VP3 wt P1 or P2 were grown in 6-well plates. After 12 h of plating, cells were incubated for 60 min with 1 mg/ml of 10-kDa Dx-Alexa Fluor 488 in serum-free DMEM. Cells were washed three times with PBS, harvested with 1 $\times$  trypsin, and blocked with 1 $\times$  DMEM–10% FBS before centrifugation of the cells at  $200 \times g$  for 5 min. Cellular pellets were washed with PBS and fixed with 4% PFA at RT for 15 min. Finally, the cells were resuspended in PBS for FACS analysis using a BD FACSAria III. Histograms were regenerated using Flow Jo 7.0.2 software.

**Flow cytometry.** Cell monolayers were harvested by trypsin treatment and blocked with DMEM–10% FBS before centrifugation of the cells at  $75 \times g$  for 5 min. Cellular pellets were washed with PBS and fixed with 4% PFA at RT for 15 min. The cells were permeabilized with 0.05% saponin in PBS containing 0.2% BSA at RT for 20 min, blocked with 10% FBS for 20 min at RT, and then incubated with anti-VP3 primary antibodies for 1 h 30 min at RT. After washes with PBS, cells were incubated with secondary antibodies conjugated with Alexa Fluor 488 for 1 h 30 min, followed by washes in PBS. The cells were suspended in PBS for FACS analysis using the BD FACSAria III. Histograms were regenerated using Flow Jo 7.0.2 software.

**Time course analysis of stable cell line growth rates.** Stable cell lines were plated on 24-well plates at a density of  $1.8 \times 10^5$  cells/well in maintenance medium containing DMEM–10% FBS and 0.5 mg/ml of G418 without penicillin-streptomycin. Twelve hours after seeding, a time point we considered 0 h, cells were washed twice with PBS, harvested, and counted employing a Neubauer chamber at 0, 6, 12, 24, and 48 h in cell culture. The number of cells was expressed as cells per milliliter.

**SDS-PAGE and Western blotting.** Protein extracts were mixed with Laemmli sample buffer and heated at  $95^{\circ}\text{C}$  for 10 min. Electrophoresis was performed on 10% polyacrylamide gels, and then the separated proteins were transferred to Hybond-ECL (GE Healthcare Argentina) nitrocellulose membranes. The membranes were blocked with blocking solution (5% nonfat milk in PBS) ON at  $4^{\circ}\text{C}$  and washed twice with PBS prior to incubation with anti-VP3, anti-VP2, anti- $\beta$ -tubulin, anti- $\beta$ -actin, anti-pan-cadherin, or anti-GAPDH primary antibodies ON at  $4^{\circ}\text{C}$ . After three washings with PBS–0.05% Tween 20, membranes were incubated with the corresponding HRP-conjugated secondary antibodies. Finally, membranes were extensively washed with PBS–0.05% Tween 20 and the corresponding immunoreactive bands were detected using an enhanced chemiluminescence detection kit from Millipore (Argentina). Data were collected with a LAS-4000 imaging system (Fujifilm, Japan) or a ChemiDoc XRS+ system (Bio-Rad, Canada). The intensities of protein bands from three independent experiments were quantified with Adobe Photoshop CS5 software.

**Indirect immunofluorescence.** QM7 or HeLa cells were grown on coverslips in a 24-well plate, and at the desired times postinfection or posttransfection (p.t.), monolayers were washed twice with PBS and the cells were fixed with a 4% PFA solution in PBS for 15 min at RT. Subsequently, cells were permeabilized with 0.05% saponin in PBS containing 0.2% BSA and then incubated with primary antibodies for 1 h 30 min at RT or ON at  $4^{\circ}\text{C}$  and with the corresponding Alexa Fluor 488- or Cy3-conjugated secondary antibodies for 1 h 30 min at RT. Finally, the monolayers were mounted with Mowiol or Mowiol plus Hoechst and analyzed by CLSM. Images were captured using an Olympus Fluoview TM FV1000 confocal microscope (Olympus, Argentina) with FV10-ASW (version 01.07.00.16) software or with a Nikon C1 confocal microscope system and the EZ-C1 program (Nikon, Japan) and processed by using Adobe CS5 (Adobe Systems).

**Statistical analysis.** Student's *t* test was performed using the Ky-Plot software version 2.0 beta 15. Values are given as the mean of triplicates  $\pm$  standard deviations (SD).

## ACKNOWLEDGMENTS

We sincerely appreciate José F. Rodríguez for generously providing reagents, expertise, and scientific discussion. We are grateful to Néstor Guerrero from the Centre de Physiopathologie (Toulouse, France) and Javier Magadán from the IHEM (Mendoza, Argentina) for sharing important reagents. We appreciate Sergio Milone and Stella Galfré from the Universidad Juan Agustín Maza for valuable laboratory aid. We appreciate Martin Sapp and Stephen A. Di Giuseppe from the Department of Microbiology and Immunology at Louisiana State University Health Sciences Center (Shreveport, LA) for generously sharing tips regarding the selective permeabilization protocol and Celina Amaya and Mariana Troncoso from the IHEM for kindly helping with the cell fractionation protocol. We thank Alejandra Medero and Rodrigo Militello for valuable technical assistance in cell culture and Elisa Bocanegra, Norberto Domizio, and Jorge Ibañez, all from the IHEM, for valuable technique assistance in CLSM handling. We also appreciate the support we received from Clara García Samartino with FACS analysis. We thank the Centre for Neurobiology of Stress at the University of Toronto at Scarborough for the use of the imaging facilities. We thank Justice F. Igweze for helping us in the final English revision of the manuscript.

This work was partially supported by funds from the Agencia Nacional de Promoción Científica y Tecnológica (MINCYT, PICT 2016-0528), SeCTyP 2013-2015 M006, and SeCTyP 2016-2018 M029 (Universidad Nacional de Cuyo) to L.R.D., PIP-CONICET 2015-2017 (112 20150100114 CO) to L.R.D. and F.A.Z., and Universidad Juan Agustín Maza (resolution 889/12, 7-11-2011) to L.R.D.

M.R.T. is supported by an NSERC Discovery grant.

## REFERENCES

- Delgui LR, Colombo MI. 2017. A novel mechanism underlying the innate immune response induction upon viral-dependent replication of host cell mRNA: a mistake of +sRNA viruses' replicases. *Front Cell Infect Microbiol* 7:5. <https://doi.org/10.3389/fcimb.2017.00005>.
- Pesavento JB, Crawford SE, Estes MK, Prasad BVV. 2006. Rotavirus proteins: structure and assembly. *Curr Top Microbiol Immunol* 309: 189–219.
- Estes MGH. 2013. Rotaviruses, p 1347–1401. In Fields BN, Knipe DM, Howley PM, Cohen JI, Griffin DE, Lamb RA, Martin MA, Racaniello VR, Roizman B (ed), *Fields virology*, 6th ed. Lippincott Williams & Wilkins, Philadelphia, PA.
- Mertens PP, Diprose J. 2004. The bluetongue virus core: a nano-scale transcription machine. *Virus Res* 101:29–43. <https://doi.org/10.1016/j.virusres.2003.12.004>.
- McDonald SM, Patton JT. 2011. Rotavirus VP2 core shell regions critical for viral polymerase activation. *J Virol* 85:3095–3105. <https://doi.org/10.1128/JVI.02360-10>.
- Giambone JJ, Donahoe JP, Dawe DL, Eidson CS. 1977. Specific suppression of the bursa-dependent immune system of chicks with infectious bursal disease virus. *Am J Vet Res* 38:581–583.
- Cosgrove AS. 1962. An apparently new disease of chickens: avian nephrosis. *Avian Dis* 6:385. <https://doi.org/10.2307/1587909>.
- Coulbaly F, Chevalier C, Gutsche I, Pous J, Navaza J, Bressanelli S, Delmas B, Rey FA. 2005. The birnavirus crystal structure reveals structural relationships among icosahedral viruses. *Cell* 120:761–772. <https://doi.org/10.1016/j.cell.2005.01.009>.
- Böttcher B, Kiselev NA, Stel'Mashchuk VY, Perevozchikova NA, Borisov AV, Crowther RA. 1997. Three-dimensional structure of infectious bursal disease virus determined by electron cryomicroscopy. *J Virol* 71: 325–330.
- Gimenez MC, Rodríguez Aguirre JF, Colombo MI, Delgui LR. 2015. Infectious bursal disease virus uptake involves macropinocytosis and trafficking to early endosomes in a Rab5-dependent manner. *Cell Microbiol* 17:988–1007. <https://doi.org/10.1111/cmi.12415>.
- Delgui LR, Rodríguez JF, Colombo MI. 2013. The endosomal pathway and the Golgi complex are involved in the infectious bursal disease virus life cycle. *J Virol* 87:8993–9007. <https://doi.org/10.1128/JVI.03152-12>.
- Méndez F, Romero N, Cubas LL, Delgui LR, Rodríguez D, Rodríguez JF. 2017. Non-lytic egression of infectious bursal disease virus (IBDV) particles from infected cells. *PLoS One* 12:e0170080. <https://doi.org/10.1371/journal.pone.0170080>.
- Lejal N, Da Costa B, Huet JC, Delmas B. 2000. Role of Ser-652 and Lys-692 in the protease activity of infectious bursal disease virus VP4 and identification of its substrate cleavage sites. *J Gen Virol* 81:983–992. <https://doi.org/10.1099/0022-1317-81-4-983>.
- Irigoyen N, Castón JR, Rodríguez JF. 2012. Host proteolytic activity is necessary for infectious bursal disease virus capsid protein assembly. *J Biol Chem* 287:24473–24482. <https://doi.org/10.1074/jbc.M112.356113>.
- Saugar I, Luque D, Oña A, Rodríguez JF, Carrascosa JL, Trus BL, Castón JR. 2005. Structural polymorphism of the major capsid protein of a double-stranded RNA virus: an amphipathic  $\alpha$  helix as a molecular switch. *Structure* 13:1007–1017. <https://doi.org/10.1016/j.str.2005.04.012>.
- Da Costa B, Chevalier C, Henry C, Huet J-C, Petit S, Lepault J, Boot H, Delmas B. 2002. The capsid of infectious bursal disease virus contains several small peptides arising from the maturation process of pVP2. *J Virol* 76:2393–2402. <https://doi.org/10.1128/JVI.76.5.2393-2402.2002>.
- Galloux M, Libersou S, Morellet N, Bouaziz S, Da Costa B, Ouldali M, Lepault J, Delmas B. 2007. Infectious bursal disease virus, a non-enveloped virus, possesses a capsid-associated peptide that deforms and perforates biological membranes. *J Biol Chem* 282:20774–20784. <https://doi.org/10.1074/jbc.M701048200>.
- Luque D, Rivas G, Alfonso C, Carrascosa JL, Rodríguez JF, Castón JR. 2009. Infectious bursal disease virus is an icosahedral polyphosphorylated dsRNA virus. *Proc Natl Acad Sci U S A* 106:2148–2152. <https://doi.org/10.1073/pnas.0808498106>.
- von Einem U, Gorbalenya AE, Schirmmeier H, Behrens S-E, Letzel T, Mundt E. 2004. VP1 of infectious bursal disease virus is an RNA-dependent RNA polymerase. *J Gen Virol* 85:2221–2229. <https://doi.org/10.1099/vir.0.19772-0>.
- Dalton RM, Rodríguez JF. 2014. Rescue of infectious birnavirus from recombinant ribonucleoprotein complexes. *PLoS One* 9:e87790. <https://doi.org/10.1371/journal.pone.0087790>.
- Ahlquist P. 2005. Virus evolution: fitting lifestyles to a T. *Curr Biol* 15:R465–R467. <https://doi.org/10.1016/j.cub.2005.06.016>.
- Schwartz M, Chen J, Janda M, Sullivan M, den Boon J, Ahlquist P. 2002. A positive-strand RNA virus replication complex parallels form and function of retrovirus capsids. *Mol Cell* 9:505–514. [https://doi.org/10.1016/S1097-2765\(02\)00474-4](https://doi.org/10.1016/S1097-2765(02)00474-4).

23. Casañas A, Navarro A, Ferrer-Orta C, González D, Rodríguez JF, Verdager N. 2008. Structural insights into the multifunctional protein VP3 of birnaviruses. *Structure* 16:29–37. <https://doi.org/10.1016/j.str.2007.10.023>.
24. Maraver A, Oña A, Abaitua F, González D, Clemente R, Ruiz-Díaz JA, Castón JR, Pazos F, Rodríguez JF. 2003. The oligomerization domain of VP3, the scaffolding protein of infectious bursal disease virus, plays a critical role in capsid assembly. *J Virol* 77:6438–6449. <https://doi.org/10.1128/JVI.77.11.6438-6449.2003>.
25. Saugar I, Irigoyen N, Luque D, Carrascosa JL, Rodríguez JF, Castón JR. 2010. Electrostatic interactions between capsid and scaffolding proteins mediate the structural polymorphism of a double-stranded RNA virus. *J Biol Chem* 285:3643–3650. <https://doi.org/10.1074/jbc.M109.075994>.
26. Oña A, Luque D, Abaitua F, Maraver A, Castón JR, Rodríguez JF. 2004. The C-terminal domain of the pVP2 precursor is essential for the interaction between VP2 and VP3, the capsid polypeptides of infectious bursal disease virus. *Virology* 322:135–142. <https://doi.org/10.1016/j.virol.2004.01.025>.
27. Garriga D, Navarro A, Querol-Audi J, Abaitua F, Rodríguez JF, Verdager N. 2007. Activation mechanism of a noncanonical RNA-dependent RNA polymerase. *Proc Natl Acad Sci U S A* 104:20540–20545. <https://doi.org/10.1073/pnas.0704447104>.
28. Lombardo E, Maraver A, Castón JR, Rivera J, Fernández-Arias A, Serrano A, Carrascosa JL, Rodríguez JF. 1999. VP1, the putative RNA-dependent RNA polymerase of infectious bursal disease virus, forms complexes with the capsid protein VP3, leading to efficient encapsidation into virus-like particles. *J Virol* 73:6973–6983.
29. van Cleef KWR, van Mierlo JT, Miesen P, Overheul GJ, Fros JJ, Schuster S, Marklewitz M, Pijlman GP, Junglen S, van Rij RP. 2014. Mosquito and *Drosophila* entomobirnaviruses suppress dsRNA- and siRNA-induced RNAi. *Nucleic Acids Res* 42:8732–8744. <https://doi.org/10.1093/nar/gku528>.
30. Valli A, Busnadiago I, Maliogka V, Ferrero D, Castón JR, Rodríguez JF, García JA. 2012. The VP3 factor from viruses of Birnaviridae family suppresses RNA silencing by binding both long and small RNA duplexes. *PLoS One* 7:e45957. <https://doi.org/10.1371/journal.pone.0045957>.
31. Chevalier C, Galloux M, Pous J, Henry C, Denis J, Da Costa B, Navaza J, Lepault J, Delmas B. 2005. Structural peptides of a nonenveloped virus are involved in assembly and membrane translocation. *J Virol* 79:12253–12263. <https://doi.org/10.1128/JVI.79.19.12253-12263.2005>.
32. Marshansky V, Futai M. 2008. The V-type H<sup>+</sup>-ATPase in vesicular trafficking: targeting, regulation and function. *Curr Opin Cell Biol* 20:415–426. <https://doi.org/10.1016/j.ceb.2008.03.015>.
33. Yoshimori T, Yamamoto A, Moriyamas Y, Futais M, Tashiroq Y. 1991. Bafilomycin A1, a specific inhibitor of vacuolar-type H<sup>+</sup>-ATPase, inhibits acidification and protein degradation in lysosomes of cultured cells. *J Biol Chem* 266:17707–17712.
34. Gómez-Sánchez R, Pizarro-Estrella E, Yakhine-Diop SMS, Rodríguez-Arribas B, Bravo-San Pedro JM, Fuentes JM, González-Polo RA. 2015. Routine Western blot to check autophagic flux: cautions and recommendations. *Anal Biochem* 477:13–20. <https://doi.org/10.1016/j.ab.2015.02.020>.
35. Jiang P, Mizushima N. 2015. LC3- and p62-based biochemical methods for the analysis of autophagy progression in mammalian cells. *Methods* 75:13–18. <https://doi.org/10.1016/j.ymeth.2014.11.021>.
36. Mizushima N, Yoshimori T. 2007. How to interpret LC3 immunoblotting. *Autophagy* 3:542–545. <https://doi.org/10.4161/auto.4600>.
37. Vitelli R, Santillo M, Lattero D, Chiariello M, Bifulco M, Bucci C. 1997. Role of the small GTPase Rab7 in the late endocytic pathway. *J Biol Chem* 272:4391–4397. <https://doi.org/10.1074/jbc.272.7.4391>.
38. Mukhopadhyay A, Funato K, Stahl PD. 1997. Rab7 regulates transport from early to late endocytic compartments in *Xenopus* oocytes. *J Biol Chem* 272:13055–13059. <https://doi.org/10.1074/jbc.272.20.13055>.
39. Gorvel JP, Chavrier P, Zerial M, Gruenberg J. 1991. rab5 controls early endosome fusion in vitro. *Cell* 64:915–925. [https://doi.org/10.1016/0092-8674\(91\)90316-Q](https://doi.org/10.1016/0092-8674(91)90316-Q).
40. Stenmark H, Parton RG, Steele-Mortimer O, Lütcke A, Gruenberg J, Zerial M. 1994. Inhibition of rab5 GTPase activity stimulates membrane fusion in endocytosis. *EMBO J* 13:1287–1296.
41. Matevossian A, Resh MD. 2015. Membrane topology of hedgehog acyl-transferase. *J Biol Chem* 290:2235–2243. <https://doi.org/10.1074/jbc.M114.625764>.
42. DiGiuseppe S, Keiffer TR, Bienkowska-Haba M, Luszczek W, Guion LGM, Müller M, Sapp M. 2015. Topography of the human papillomavirus minor capsid protein L2 during vesicular trafficking of infectious entry. *J Virol* 89:10442–10452. <https://doi.org/10.1128/JVI.01588-15>.
43. Choe SS, Kirkegaard K. 2004. Intracellular topology and epitope shielding of poliovirus 3A protein. *J Virol* 78:5973–5982. <https://doi.org/10.1128/JVI.78.11.5973-5982.2004>.
44. Krawczyk E, Suprynowicz FA, Sudarshan SR, Schlegel R. 2010. Membrane orientation of the human papillomavirus type 16 E5 oncoprotein. *J Virol* 84:1696–1703. <https://doi.org/10.1128/JVI.01968-09>.
45. Labay V, Weichert RM, Makishima T, Griffith AJ. 2010. Topology of transmembrane channel-like gene 1 protein. *Biochemistry* 49:8592–8598. <https://doi.org/10.1021/bi1004377>.
46. Braakman I, Hebert DN. 2013. Protein folding in the endoplasmic reticulum. *Cold Spring Harb Perspect Biol* 5:a013201. <https://doi.org/10.1101/cshperspect.a013201>.
47. Joyce CW, Shelness GS, Davis MA, Lee RG, Skinner K, Anderson RA, Rudel LL. 2000. ACAT1 and ACAT2 membrane topology segregates a serine residue essential for activity to opposite sides of the endoplasmic reticulum membrane. *Mol Biol Cell* 11:3675–3687. <https://doi.org/10.1091/mbc.11.11.3675>.
48. Rodríguez JM, García-Escudero R, Salas ML, Andrés G. 2004. African swine fever virus structural protein p54 is essential for the recruitment of envelope precursors to assembly sites. *J Virol* 78:4299–1313. <https://doi.org/10.1128/JVI.78.8.4299-4313.2004>.
49. Stevanovic A, Thiele C. 2013. Monotopic topology is required for lipid droplet targeting of ancient ubiquitously protein 1. *J Lipid Res* 54:503–513. <https://doi.org/10.1194/jlr.M033852>.
50. Nakamura N, Rabouille C, Watson R, Nilsson T, Hui N, Slusarewicz P, Kreis TE, Warren G. 1995. Characterization of a cis-Golgi matrix protein, GM130. *J Cell Biol* 131:1715–1726. <https://doi.org/10.1083/jcb.131.6.1715>.
51. Gao YS, Alvarez C, Nelson DS, Sztul E. 1998. Molecular cloning, characterization, and dynamics of rat formiminotransferase cyclodeaminase, a Golgi-associated 58-kDa protein. *J Biol Chem* 273:33825–33834. <https://doi.org/10.1074/jbc.273.50.33825>.
52. Mertens J, Casado S, Mata CP, Hernando-Pérez M, de Pablo PJ, Carrascosa JL, Castón JR. 2015. A protein with simultaneous capsid scaffolding and dsRNA-binding activities enhances the birnavirus capsid mechanical stability. *Sci Rep* 5:13486. <https://doi.org/10.1038/srep13486>.
53. Goldenberg NM, Steinberg BE. 2010. Surface charge: a key determinant of protein localization and function. *Cancer Res* 70:1277–1280. <https://doi.org/10.1158/0008-5472.CAN.09-2905>.
54. Waterhouse AM, Procter JB, Martin DMA, Clamp M, Barton GJ. 2009. Jalview version 2—a multiple sequence alignment editor and analysis workbench. *Bioinformatics* 25:1189–1191. <https://doi.org/10.1093/bioinformatics/btp033>.
55. Sharma M, Naslavsky N, Caplan S. 2008. A role for EHD4 in the regulation of early endosomal transport. *Traffic* 9:995–1018. <https://doi.org/10.1111/j.1600-0854.2008.00732.x>.
56. Tristan C, Shahani N, Sedlak TW, Sawa A. 2011. The diverse functions of GAPDH: views from different subcellular compartments. *Cell Signal* 23:317–323. <https://doi.org/10.1016/j.cellsig.2010.08.003>.
57. Delgui L, González D, Rodríguez JF. 2009. Infectious bursal disease virus persistently infects bursal B-lymphoid DT40 cells. *J Gen Virol* 90:1148–1152. <https://doi.org/10.1099/vir.0.008870-0>.
58. Chavrier P, Parton RG, Hauri HP, Simons K, Zerial M. 1990. Localization of low molecular weight GTP binding proteins to exocytic and endocytic compartments. *Cell* 62:317–329. [https://doi.org/10.1016/0092-8674\(90\)90369-P](https://doi.org/10.1016/0092-8674(90)90369-P).
59. Mu FT, Callaghan JM, Steele-Mortimer O, Stenmark H, Parton RG, Campbell PL, McCluskey J, Yeo JP, Tock EPC, Toh BH. 1995. EEA1, an early endosome-associated protein: EEA1 is a conserved  $\alpha$ -helical peripheral membrane protein flanked by cysteine “fingers” and contains a calmodulin-binding IQ motif. *J Biol Chem* 270:13503–13511. <https://doi.org/10.1074/jbc.270.22.13503>.
60. Diaz-Salinas MA, Silva-Ayala D, Lopez S, Arias CF. 2014. Rotaviruses reach late endosomes and require the cation-dependent mannose-6-phosphate receptor and the activity of cathepsin proteases to enter the cell. *J Virol* 88:4389–4402. <https://doi.org/10.1128/JVI.03457-13>.
61. Stenmark H. 2009. Rab GTPases as coordinators of vesicle traffic. *Nat Rev Mol Cell Biol* 10:513–525. <https://doi.org/10.1038/nrm2728>.
62. White J, Matlin K, Helenius A. 1981. Cell fusion by Semliki Forest, influenza, and vesicular stomatitis viruses. *J Cell Biol* 89:674–679. <https://doi.org/10.1083/jcb.89.3.674>.
63. Garriga D, Querol-Audi J, Abaitua F, Saugar I, Pous J, Verdager N,

- Castón JR, Rodríguez JF. 2006. The 2.6-angstrom structure of infectious bursal disease virus-derived T=1 particles reveals new stabilizing elements of the virus capsid. *J Virol* 80:6895–6905. <https://doi.org/10.1128/JVI.00368-06>.
64. De Craene J-O, Bertazzi DL, Bär S, Friant S. 2017. phosphoinositides, major actors in membrane trafficking and lipid signaling pathways. *Int J Mol Sci* 18:634. <https://doi.org/10.3390/ijms18030634>.
  65. Di Paolo G, De Camilli P. 2006. Phosphoinositides in cell regulation and membrane dynamics. *Nature* 443:651–657. <https://doi.org/10.1038/nature05185>.
  66. McLaughlin S. 1989. The electrostatic properties of membranes. *Annu Rev Biophys Chem* 18:113–136. <https://doi.org/10.1146/annurev.bb.18.060189.000553>.
  67. Olivetto M, Arcangeli A, Carlá M, Wanke E. 1996. Electric fields at the plasma membrane level: a neglected element in the mechanisms of cell signalling. *Bioessays* 18:495–504. <https://doi.org/10.1002/bies.950180612>.
  68. Balla T. 2005. Inositol-lipid binding motifs: signal integrators through protein-lipid and protein-protein interactions. *J Cell Sci* 118:2093–2104. <https://doi.org/10.1242/jcs.02387>.
  69. Takenawa T, Itoh T. 2006. Membrane targeting and remodeling through phosphoinositide-binding domains. *IUBMB Life* 58:296–303.
  70. Stachowiak JC, Brodsky FM, Miller EA. 2013. A cost–benefit analysis of the physical mechanisms of membrane curvature. *Nat Cell Biol* 15: 1019–1027. <https://doi.org/10.1038/ncb2832>.
  71. Kirchhausen T. 2012. Bending membranes. *Nat Cell Biol* 14:906–908. <https://doi.org/10.1038/ncb2570>.
  72. Delgui L, Oña A, Gutiérrez S, Luque D, Navarro A, Castón JR, Rodríguez JF. 2009. The capsid protein of infectious bursal disease virus contains a functional  $\alpha 4\beta 1$  integrin ligand motif. *Virology* 386:360–372. <https://doi.org/10.1016/j.virol.2008.12.036>.
  73. Gorbalenya AE, Koonin EV, Donchenko AP, Blinov VM. 1988. A novel superfamily of nucleoside triphosphate-binding motif containing proteins which are probably involved in duplex unwinding in DNA and RNA replication and recombination. *FEBS Lett* 235:16–24. [https://doi.org/10.1016/0014-5793\(88\)81226-2](https://doi.org/10.1016/0014-5793(88)81226-2).
  74. Adams MJ, Carstens EB. 2012. Ratification vote on taxonomic proposals to the International Committee on Taxonomy of Viruses (2012). *Arch Virol* 157:1411–1422. <https://doi.org/10.1007/s00705-012-1299-6>.
  75. Gorbalenya AE, Koonin EV. 1988. Birnavirus RNA polymerase is related to polymerases of positive strand RNA viruses. *Nucleic Acids Res* 16:7735. <https://doi.org/10.1093/nar/16.15.7735>.
  76. Pan J, Vakharia VN, Tao YJ. 2007. The structure of a birnavirus polymerase reveals a distinct active site topology. *Proc Natl Acad Sci U S A* 104:7385–7390. <https://doi.org/10.1073/pnas.0611599104>.
  77. Johnson JE, Munshi S, Liljas L, Agrawal D, Olson NH, Reddy V, Fisher A, McKinney B, Schmidt T, Baker TS. 1994. Comparative studies of T=3 and T=4 icosahedral RNA insect viruses. *Arch Virol Suppl* 9:497–512.
  78. Ertel KJ, Benefield D, Castaño-Diez D, Pennington JG, Horswill M, den Boon JA, Otegui MS, Ahlquist P. 2017. Cryo-electron tomography reveals novel features of a viral RNA replication compartment. *Elife* 6:25940. <https://doi.org/10.7554/eLife.25940>.
  79. Fernández-Arias A, Risco C, Martínez S, Albar JP, Rodríguez JF. 1998. Expression of ORF A1 of infectious bursal disease virus results in the formation of virus-like particles. *J Gen Virol* 79:1047–1054. <https://doi.org/10.1099/0022-1317-79-5-1047>.
  80. Lin T-W, Lo C-W, Lai S-Y, Fan R-J, Lo C-J, Chou Y-m., Thiruvengadam R, Wang AH-J, Wang M-Y. 2007. Chicken heat shock protein 90 is a component of the putative cellular receptor complex of infectious bursal disease virus. *J Virol* 81:8730–8741. <https://doi.org/10.1128/JVI.00332-07>.